



NTNU – Trondheim
Norwegian University of
Science and Technology

Laboratory Measurements of Ice-Concrete Abrasion with Different Types of Ice Quality

Nicolai Seggaard Greaker

Civil and Environmental Engineering

Submission date: June 2014

Supervisor: Knut Vilhelm Høyland, BAT

Co-supervisor: Stefan Jacobsen, IKT

Norwegian University of Science and Technology
Department of Civil and Transport Engineering



Report Title: Laboratory Measurements of Ice-Concrete Abrasion with Different Types of Ice Quality	Date: 10.06.14
	Number of pages (incl. appendices): 118
	Master Thesis <input checked="" type="checkbox"/> Project Work <input type="checkbox"/>
Name: Nicolai Seggaard Greaker	
Professor in charge/supervisor: Knut Vilhelm Høyland	
Other external professional contacts/supervisors: Stafan Jacobsen	

<p>Abstract</p> <p>Ice-concrete abrasion has been investigated by review of lab- and field studies and by laboratory testing. The specific objective of this thesis has been to investigate the possible effects of different ice qualities on laboratory ice-concrete abrasion tests. This has been done by altering the ice parameters and keeping other test conditions constant.</p> <p>Five procedures have been developed to produce ice with differing qualities. Thin sections from each procedure have been investigated and showed distinguishable ice texture. Large grains with vertical growth were observed for ice made in FRYISIS, a water tank located at NTNU. Small grain sizes and ice texture similar to that of sea ice was seen for ice made by freezing water in a plexiglas tube at -20 °C and blended with slush. Ice density and porosity was measured by applying Archimedes law, with cooled kerosene used as fluid. The highest porosity was measured for ice samples made by freezing carbonated water in a sealed tube, $\phi = 17.0\%$. The lowest porosity was measured for the ice samples made in FRYISIS, $\phi = 0.9\%$.</p> <p>Earlier studies on ice-concrete abrasion have been reviewed and have shown that test set-up conditions and results are varying. It has been concluded that in order to obtain results with a satisfying accuracy, concrete samples should be abraded to a minimum depth of 0.05 mm</p> <p>The measurement set-up for measuring abrasion depth was investigated and concluded to be repeatable. Of the two presented methods to calculate abrasion rate, it was concluded that referring ice exposed grid points to their nearest reference point was the most accurate. The abrasion rates obtained from the five different ice procedures varied in the same range as the abrasion rates for different concrete samples. Mean abrasion rate measured in this thesis varied in the range $\approx 0.02 - 0.07$ mm/km. Lowest mean abrasion rate was measured for ice that did not crush during the abrasion test. Highest abrasion rate was measured for the ice made in FRYISIS, (0.086 ± 0.086) mm/km.</p>
--

Keywords:

1. Ice-Concrete Abrasion
2. Ice Properties
3. Concrete Technology
4. Laboratory Testing

Abstract

Ice-concrete abrasion has been investigated by review of lab- and field studies and by laboratory testing. The specific objective of this thesis has been to investigate the possible effects of different ice qualities on laboratory ice-concrete abrasion tests. This has been done by altering the ice parameters and keeping other test conditions constant.

Five procedures have been developed to produce ice with differing qualities. Thin sections from each procedure have been investigated and showed distinguishable ice texture. Large grains, $>10 \times 7$ cm, with vertical growth were observed for ice made in FRYISIS, a water tank located at NTNU. Small grain sizes and ice texture similar to that of sea ice was seen for ice made by freezing water in a plexiglas tube at -20 °C and blended with slush. Ice density and porosity was measured by applying Archimedes law, with cooled kerosene used as fluid. The highest porosity was measured for ice samples made by freezing carbonated water in a sealed tube, $\phi = 17.0$ %. The lowest porosity was measured for the ice samples made in FRYISIS, $\phi = 0.9$ %.

Earlier studies on ice-concrete abrasion have been reviewed and have shown that test set-up conditions and results are varying. It has been concluded that in order to obtain results with a satisfying accuracy, concrete samples should be abraded to a minimum depth of 0.05 mm

The measurement set-up for measuring abrasion depth was investigated and concluded to be repeatable. Of the two presented methods to calculate abrasion rate, it was concluded that referring ice exposed grid points to their nearest reference point was the most accurate. The abrasion rates obtained from the five different ice procedures varied in the same range as the abrasion rates for different concrete samples. Mean abrasion rate measured in this thesis varied in the range $\approx 0.02 - 0.07$ mm/km. Lowest mean abrasion rate was measured for ice that did not crush during the abrasion test. Highest abrasion rate was measured for the ice made in FRYISIS, (0.086 ± 0.086) mm/km.

Acknowledgements

I would like to express my sincerest gratitude to prof. Knut V. Høyland and prof. Stefan Jacobsen. I have benefited greatly from their expertise, guidance, constructive discussions and feedback.

I wish to thank Kristian Sætre for the academic exchanges, discussions and help measuring the density and porosity of the ice samples. It has been comforting not having to cope with the many challenges of the abrasion rig by my self. Recognition is also given to Anna Pustogvar for all the constructive help she has provided me. I would like to express my gratitude to Thor Olav Myklebust for showing me how to operate the freezing tank FRYSSIS. The motivation and help I have received from Cathrine Y. Pederesn is dearly appreciated. Thank you all.

I also owe a great thanks to Steinar Seehuus and his colleagues at the NTNU concrete laboratory for overviewing operations of the abrasion rig. Without them, there would have been no abrasion results to show for. They have all been very helpful and determined to keep the abrasion rig operational. Steinar is also to be thanked for showing me how to perform compression tests and how to prepare the concrete samples. Terje Petersen did a great job making the cylinders I needed.

Last but not least, I want to thank my loving family and friends. A special mention goes to my late grandfather, Jan Greaker, who would have been very proud to see the day I submitted this work.

Nicolai Seggaard Greaker
Trondheim, 10/6 2014

Contents

1	Introduction	1
1.1	Background	1
1.2	Objective	2
1.3	Scope	2
1.4	Structure of Thesis	2
2	Theory	3
2.1	Ice	3
2.1.1	Formation of Ice	3
2.1.2	Crystal Structure of Ih Ice	4
2.1.3	Ice Growth	4
2.1.4	Ice Classification	5
2.1.5	Sea Ice	6
2.1.6	Ice Density	8
2.1.7	Mechanical Properties of Ice	8
2.2	Concrete	12
2.2.1	Characteristic Strength	12
2.2.2	Effect of Temperature	12
2.2.3	Profile Roughness	13
2.3	Wear	14
2.3.1	Abrasion Mechanism	14
2.3.2	Abrasion Variables	15
2.3.3	Abrasion Models	17
3	Experimental Set-up and Procedures	18
3.1	Ice Samples	18
3.1.1	Procedure 1 - Plexiglas Tube	18
3.1.2	Procedure 2 - POM Tube	19
3.1.3	Procedure 3 - Agitated Water	20
3.1.4	Procedure 4 - Porous Ice	20
3.1.5	Procedure 5 - FRYISIS	22
3.2	Thin Sections	23
3.3	Density and Porosity Measurements	23
3.4	Concrete Samples	25

3.4.1	Sample Preparation	25
3.4.2	Concrete Density	26
3.4.3	Concrete Strength	27
3.5	Ice-Concrete Abrasion Rig	28
3.5.1	Modifications	30
3.5.2	Test Conditions	31
3.6	Measurements	32
3.6.1	Abrasion Depth	32
3.6.2	Abrasion Rate	33
3.6.3	Presentation of Conducted Abrasion Experiment	35
3.7	Calibrations	36
3.7.1	Effective Sliding Distance	36
3.7.2	Chord Calibration	36
3.7.3	Thermal Expansion	36
3.8	Analysis of earlier Ice Abrasion Results	37
4	Results	38
4.1	Ice Samples	38
4.2	Thin Sections	40
4.2.1	Thin Sections of Procedure 1 - Plexiglas Tube	40
4.2.2	Thin Sections of Procedure 2 - POM Tube	42
4.2.3	Thin Sections of Procedure 3 - Agitated Water	43
4.2.4	Thin Sections of Procedure 4 -Porous Ice	45
4.2.5	Thin Sections of Procedure 5 - FRYSIS	46
4.3	Ice Density and Porosity	48
4.4	Concrete Strength and Density	49
4.5	Analysis of earlier Ice Abrasion Results	49
4.5.1	Abrasion Rate vs. Concrete Type	49
4.5.2	Abrasion Rate vs. Relative Difference	51
4.6	Abrasion Rig	53
4.6.1	Abrasion Rate	53
4.6.2	Abrasion Rate vs. Ice Quality	54
4.6.3	Profile Roughness	56
4.6.4	Concrete Samples after Ice Exposure	58
4.6.5	Friction, Load and Temperature Variation	60
5	Discussion and Analysis	64
5.1	Ice Samples	64
5.1.1	Procedure 1 vs. Pocerure 2	65
5.1.2	Mechanical Properties of Ice	67
5.1.3	Shrinkage	68
5.2	Analysis of Ice-Concrete Abrasion Studies at NTNU	69
5.2.1	Analysis of earlier Ice-Concrete Abrasion Results	70
5.3	Abrasion Measurement Set-Up and Calculation Procedure	72
5.3.1	Equipment	72
5.3.2	Accuracy of Measurement Set-Up	73

5.3.3	Calculation Method 1 vs. Method 2	73
5.4	Concrete Sample	76
5.4.1	Profile Roughness	76
5.5	Ice-Concrete Abrasion Results	78
5.5.1	Abrasion Rate Comparison	78
5.5.2	Abrasion Rate vs. Ice Quality	79
5.5.3	Effect of Volumetric Expansion	80
5.5.4	Friction histogram	81
5.5.5	Load histogram	82
5.5.6	Temperature histogram	83
6	Conclusions	84
	Bibliography	86
	Appendix	
	A MSc Thesis Template	
	B Ice Samples	
	C Ice Density and Porosity Measurements	
	D Concrete Density Measurement	
	E Mean Abrasion Rates from earlier Results	
	F Abrasion Depth Measurement Sheet	
	G Ice-Concrete Abrasion Chart	
	H Matlab Script for Abrasion Result Presentation	

List of Figures

2.1	Hexagonal Structure of Ice Ih.	4
2.2	Ice-structure interaction	5
2.3	Model of sea ice crystal structure	6
2.4	Thin section of sea and fresh water ice.	7
2.5	Compressive strength and tensile strength of ice versus temperature.	9
2.6	Compressive strength versus strain rate.	9
2.7	Young's modulus vs. porosity of cold, arctic sea ice.	10
2.8	Uniaxial compressive strength in respect to orientation	11
2.9	Sequence of events in the ice abrasion mechanism	14
3.1	The plexiglas tube	19
3.2	The POM tube	20
3.3	Preparation of ice samples with procedure 3	21
3.4	Preparation of ice samples with procedure 4	21
3.5	Experimental set-up for procedure 5	22
3.6	Procedure for making a thin section.	23
3.7	Experimental set-up for density and porosity measurements.	24
3.8	Preparation of concrete sample with saw surface.	25
3.9	Casted surface concrete sample	26
3.10	Compression test set-up	27
3.11	Ice-concrete abrasion rig	28
3.12	Details of the ice-concrete abrasion rig	29
3.13	Ice-concrete abrasion instruments	30
3.14	Automatically adjustment of table with new motor	31
3.15	Abrasion measurement set-up.	32
3.16	Predefined grid points	33
3.17	Calculation of abrasion rate with method 1.	34
3.18	Calculation of abrasion rate with method 2.	35
4.1	Ice samples	39
4.2	Thin section of sample 14 made after procedure 1.	40
4.3	Thin section of sample15 made after method 1.	41
4.4	Thin section of sample 16 made after procedure 1.	41
4.5	Thin section of sample a24 made after procedure 2.	42
4.6	Thin section of sample a25 made after procedure 2.	42

4.7	Thin section of sample a26 made after procedure 2.	43
4.8	Thin section of sample b7 made after procedure 3.	43
4.9	Thin section of sample b8 made after method 3.	44
4.10	Thin section of sample b11 made after procedure 3.	44
4.11	Thin section of sample c12 made after procedure 4.	45
4.12	Thin section of sample c13 made after procedure 4.	45
4.13	Thin section of sample c14 made after procedure 4.	46
4.14	Thin section of sample d5 made after procedure 5.	46
4.15	Thin section of sample d9 made after procedure 5.	47
4.16	Thin section of sample d22 made after procedure 5.	47
4.17	Abrasion rate vs. concrete types.	50
4.18	Relative difference vs. abrasion rate.	52
4.19	Abrasion rate vs. ice quality.	54
4.20	Comparison of the two calculation methods	55
4.21	Concrete samples after ice exposure	59
4.22	Comparison of friction	60
4.23	Comparison of friction variations after 60 min	61
4.24	Comparison of forces	62
4.25	Comparison of room temperature	63
5.1	Comparison of vertical sections during thin section preparation . . .	66
5.2	Air pillar in ice sample made after procedure 5.	67
5.3	Ice sample shrinkage	68
5.4	Mitutoyo indicator needle hanging on a cavity wall.	72
5.5	Mesh of grid points	77
5.6	Comparison of POM and 70 mm ice sample after abrasion	80
5.7	De-icing of load-cells	82
5.8	Room temperature variation with different y-axis	83

List of Tables

2.1	Summary of reviewed studies on wear variables	15
3.1	Experimental test conditions for the abrasion rig	31
4.1	Ice density and porosity	48
4.2	Concrete strength and density	49
4.3	Abrasion rates	53
4.4	Average roughness	56
4.5	Mean square root roughness	57
5.1	Comparison of ice-concrete abrasion studies at NTNU	69
5.2	Comparison of weighted standard deviations.	74

Chapter 1

Introduction

Due to the growing demand for fossil fuel, there has been an increased focus on the potential for exploiting the sub-arctic and arctic regions, in an environmentally safe manner. It is expected that large offshore oil and gas development projects relatively soon will be carried out in these regions. In order to have successful operations, the ability to work under the demanding conditions of the harsh environment is an absolute political requirement, (Gudmestad, 2013). The environment in these regions are extremely demanding. Heavy winds, high waves and drifting ice are frequently occurring events. To face these challenges, good knowledge and prediction of how these occurring events influence future installations are vital.

Concrete is a material often used in construction of marine structures, such as oil platforms, sea wind mill foundations, dams and lighthouses. If, however, concrete is exposed to moving ice, it will abrade. Precautions are therefore necessary when designing, producing and applying concrete structures for environments with ice infested waters to assure proper durability and service life. A concrete-ice abrasion laboratory has been designed and is presently in operation at the department of structural engineering at the Norwegian University of Science and Technology, NTNU. The laboratory simulates concrete-ice abrasion by forcing fresh water ice on a concrete surface while moving the ice back and forth and controlling ice pressure, average speed, temperature etc. The objective of the laboratory is to develop durable materials for ice-abraded concrete structures and to better predict service life time of such structures.

1.1 Background

There has already been published several papers discussing concrete ice abrasion at NTNU. Much of the work concerns describing and improving the abrasion rig and the involving test and measuring procedures. The importance of concrete and ice parameters on ice-concrete abrasion has been studied and concrete samples with various qualities have been tested. Internationally, research has been carried out

for some decades. Literature review shows that the findings in these researches can be contradictory. No standardized test method has been developed for ice abrasion, neither practically nor theoretically. Comparisons of different findings can therefore be challenging, even meaningless. Further knowledge on this topic seems to be needed to draw any solid conclusions. Some interesting findings were uncovered in the earlier thesis "Ice Quality in Measurements of Concrete Ice Abrasion: Pre-study", (Greaker, 2013), which was the pre-study to this thesis. The present work continuous and concludes on aspects highlighted in the earlier thesis.

1.2 Objective

The motivation is to determine whether fresh water based laboratory tests can be successfully used as tools to analyze abrasion on marine structures exposed to salt water conditions in extreme environments. The specific objective of this thesis has been to investigate the possible effects of different ice qualities on laboratory ice-concrete abrasion tests. This has been done by altering the ice parameters and keeping other test conditions constant.

1.3 Scope

Five different procedures of making ice will be developed. The differences in ice sample qualities will be determined by studying thin sections and density measurements. Measurement set-up accuracy of the abrasion rig at NTNU will be investigated and methods on how to calculate abrasion rate will be deduced. Ice-concrete abrasion experiments will be conducted on 15 concrete samples of equal quality and test conditions will be constant. As part of a quality assurance, the abrasion results obtained from the conducted experiments will be compared to the results obtained in earlier related thesis.

1.4 Structure of Thesis

At first, the principles of ice, concrete and wear is presented. This will give the reader an introduction on the complex field of ice-concrete abrasion. As next, the experiments conducted and procedures developed to achieve the objective of the thesis are thoroughly described. The results from these experiments are presented in the following chapter and will be discussed and analyzed in chapter 5. Main conclusions that can be drawn from the discussions of the results are rendered in the last chapter.

Chapter 2

Theory

2.1 Ice

The objective of the pre-study, "Ice Quality in Measurements of Concrete Ice Abrasion: Pre-study", (Greker, 2013), was to investigate the quality of ice that had been used in earlier ice-concrete abrasion related theses at NTNU. A detailed description of ice abrasion-related theory was presented in the pre-study. Theory relevant to the objective of this thesis has been rendered and supplementary theory about the ice texture is presented.

2.1.1 Formation of Ice

Ice is defined as the solid phase of water (Furukawa, 2011). To form ice, ice crystals need to be nucleated. In natural freshwater there will most often be some form of nuclei, such as dust particles, bacterias, etc., on which ice crystals can form. If no particles were at hand to initiate nucleation, water temperature could be lower than the freezing temperature of water. This phenomena is referred to as supercooling (Palmer and Croasdale, 2012). Supercooling will not be discussed further hence it rarely occurs in natural conditions. In calm water (flow velocity < 0.5 m/s) ice usually forms as spicules or plate-like crystals at the water surface, known as first ice. With time the spicules grow into a network of dendrites that eventually freeze together forming a continuous ice cover, called skim ice. Once the ice cover is formed, the ice starts to thicken as heat is removed from the ice to it's surroundings by conduction and to a small extent by radiation (Ashton, 2004) and (Palmer and Croasdale, 2012). Ice growth will be discussed further in section 2.1.3.

2.1.2 Crystal Structure of Ih Ice

For different combinations of pressure and temperature, ice can have more than 13 different crystalline phases. The most important and common phase is the hexagonal ice, termed ordinary ice by Schulson and Duval (2009). As water freezes in a temperature range 0 °C to -80 °C under normal atmospheric conditions, the water molecules are arranged in an orderly repetitive position to form a crystalline solid with hexagonal structure, known as ice Ih (Furukawa, 2011). The hexagonal structure of ice Ih can be seen in figure 2.1.

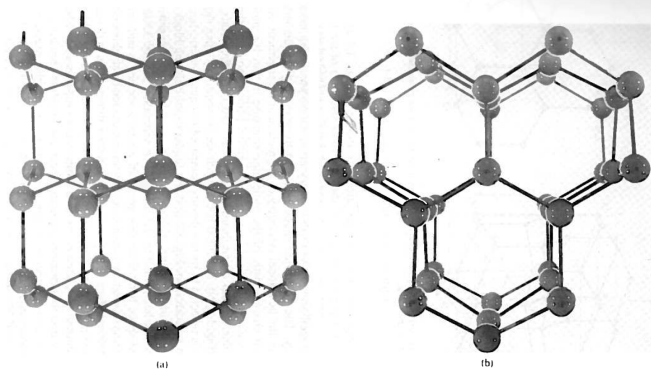


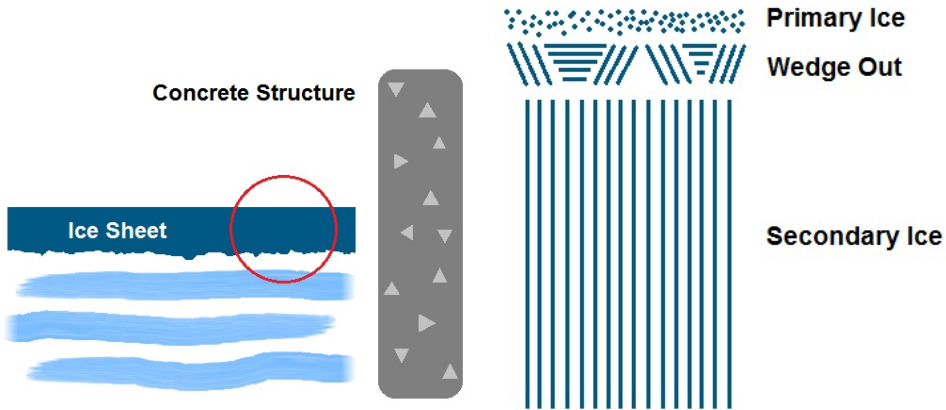
Figure 2.1: Hexagonal Structure of Ice Ih. (a) View perpendicular to the c-axis. (b) View along the c-axis. Figure from (Hobbs, 1974).

According to Hobbs (1974) the geometrical arrangement of the water molecules is such that the oxygen molecule is approximately at the center of its four neighboring hydrogen atoms. This molecular arrangement is also such that the molecules are concentrated close to a series of parallel planes known as basal planes. The normal to the basal plane is referred to as the optical axis of the crystal, also referred to as the c-axis.

2.1.3 Ice Growth

Ice formed in saline water and ice formed in fresh water are named sea ice and fresh water ice respectively. Ice is a complex material and its structure depends on environmental conditions. Fresh water ice can consist of solid ice, gas and other material that has been trapped within the ice during freezing. Sea ice can additionally consist of brine and depending upon the temperature, various types of solid salts (Timco and Weeks, 2009). Heat conduction occurs favorably at the greatest molecule concentrations. Ice growth will therefore be greatest parallel to the basal plane as the molecule concentration is greatest there, see figure 2.1. Large temperature gradients, result in rapid ice growth and small grain sizes. Low temperature gradients cause prolonged growth and large grain sizes. In the initial ice layer, the crystal structure will have random orientated c-axis. As ice growth continuous the more favorably orientated crystals will expand faster than the less

favorably orientated crystals, causing a so called "wedge out" effect, see figure 2.2b. This effect leads to a distinctive crystal structure, known as columnar ice. Columnar ice has oblong crystals standing in the ice with a horizontal orientated c-axis.



(a) Illustration of an Ice sheet approaching a concrete Structure.

(b) A close up of the red circle in 2.2a.

Figure 2.2: Ice-structure interaction

2.1.4 Ice Classification

Ashton (2004) classifies ice according to the size, shape and orientation of the crystals and the environmental factors that caused them. Relevant classifications are rendered here:

Primary ice

P1 Calm surface; small temperature gradient.

P2 Calm surface; large temperature gradient.

Secondary ice

S2 Columnar ice; preferred horizontal orientation of c-axis. Random orientation.

S3 Columnar ice; preferred aligned horizontal orientation of c-axis. One dominating direction of c-axis.

Primary ice refers to the initial ice layer formed at the water surface. This layer consists of very small grains with random orientations. The thickness of the layer varies from a few millimeters up to 15 centimeters. If ice thickness grows large, the primary ice layer is usually neglected hence the predominance of the underlying secondary ice layer. Secondary ice is a result of the wedge out effect seen in figure

2.2b. The crystals grow vertically and their diameter increases with depth. At a depth of 0.3 to 0.6 meters the diameter is frequently 5 - 15 cm (Bergdahl, 1977).

2.1.5 Sea Ice

When ice forms in saline waters, the crystal structure of ice is unaffected by the presence of salts. The reason for this is that the ice lattice is prevailed, excluding salts as freezing proceeds. Pockets of concentrated solutions are trapped within the ice structure, known as brine pockets. The entrapment of brine occurs as the thickening of ice continues, see figure 2.3. The growing SK ice planes stretch like fingers down into the underlying water. When they reach a length of approximately 2 - 3 cm, connections are formed between the fingers, thereby confining the saline water between them. The confined water, referred to as brine, will at first have a salinity approximately equal to that of the sea water. With time, the water in the brine pockets freezes, increasing the salinity of the brine as more salt is expelled. Brine voids will migrate downwards due to gravitational drainage and temperature gradients, creating so called brine channels. The presence of salts makes bulk properties of sea ice different from those of fresh water ice. A general conclusion is that sea ice is weaker than fresh water ice, (Bergdahl, 1977).

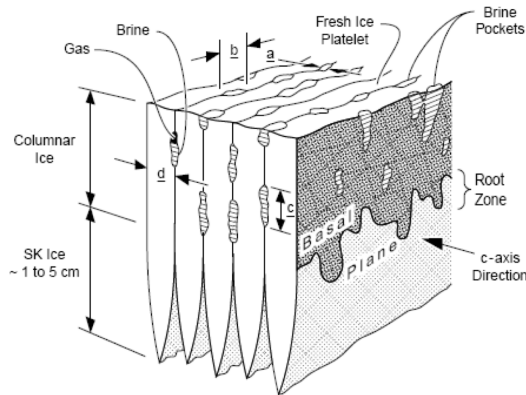
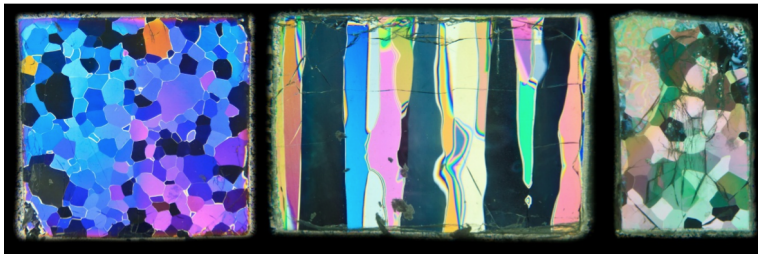


Figure 2.3: Model of sea ice crystal structure. From Marchenko (2013):

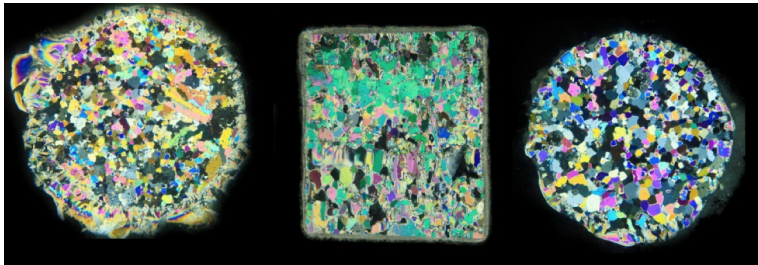
$$a \leq b \leq c$$

$$a \sim 0.1-0.3 \text{ mm}; b \sim 1-5 \times a; c > a \times 5; d \sim 0.25-1.25 \text{ mm}$$

Environmental conditions in sea- and in fresh waters influence the ice texture differently. The ice texture of fresh water ice, figure 2.4a, and sea water ice, figure 2.4b is presented in figure 2.4. The fresh water ice was retrieved from a small lake close to mine 7 in Longyearbyen, Svalbard. The sea water ice originated from an ice ridge in Van Keulen Fjord, Svalbard. By comparing the two thin sections, it is apparent that varying environmental conditions give rise to different ice texture. Larger grains with columnar growth is clearly seen for the fresh water ice. The environmental conditions in the lake can be described as calm compared to the more harsh conditions in the Van Keulen Fjord. In the fjord, wind and waves are mixing water and air continuously and causing interactions between ice sheets, resulting in smaller ice grains and a more disordered ice texture.



(a) From left; Upper horizontal, vertical and lower horizontal thin section of fresh water ice.



(b) From left; Upper horizontal, vertical and lower horizontal thin section of sea water ice.

Figure 2.4: Thin section of sea and fresh water ice. Sea ice originates from an ice ridge in Van Keulen Fjord, Svalbard and the fresh water ice from a lake close to mine 7 in Longyearbyen, Svalbard. Figure from (Greaker et al., 2012).

2.1.6 Ice Density

Density is highly correlated with the amount of void in the specimen. Pure ice is defined as ice without any gas, brine, solid salts or other impurities and its density, ρ_i , is calculate from, (Cox and Weeks, 1983):

$$\rho_i = 0.917 - 1.403 \times 10^{-4} \times T(^{\circ}\text{C}) \quad [\text{Mg}/\text{m}^3] \quad (2.1)$$

Where T is the ice sample core temperature. Pure ice is rarely found in natural conditions and the purpose of equation 2.1 is to calculate the ice porosity which will be presented in section 2.1.7. The ice density of samples containing gas, brine or other impurities can be calculated with Archimedes law:

$$\rho_{ice} = \frac{m_{ice,air}}{m_{ice,air} - m_{ice,par}} \times \rho_F \quad (2.2)$$

Where ρ_{ice} is the ice density, $m_{ice,air}$ is mass of ice, $m_{ice,par}$ is mass of the ice submerged in to a fluid and ρ_F is the density of the fluid. As the density is greatly affected by the amount of gas and/or brine, ice growth rate is essential. Rapid ice growth will confine more gas/brine, thereby lower the ice density.

2.1.7 Mechanical Properties of Ice

The mechanical properties of ice are divided into two distinctive categories; namely those related to short-term and long-term behavior. The short-term properties are related to temperature, loading rate, porosity, grain size, brine content and orientation. Long-term behavior differentiate from short-term behavior by considering load duration and deformation rate instead of loading rate. Due to the relatively short duration of the ice-concrete abrasion experiment, this thesis will be considering short-term behavior.

The load magnitude exerted on a structure by moving ice is influenced by many factors. The most important factors are temperature, porosity, brine content, strain rate, grain size and orientation (Huovinen, 1990). Hence the complexity and intervening dependence of these factors, ice mechanics is a complex topic. To get a better understanding on how the mechanical properties alter with altering factors and to be able to evaluate them, relevant factors have been rendered in the following.

Temperature

The mechanical properties of ice are to a great extent related to temperature. In natural conditions the temperature varies with the ice thickness. Ice at the surface will have a temperature approximately equal to the air temperature, while the ice at the bottom will have a temperature close to the freezing point of water. Hence air temperature fluctuates, the temperature profile in the ice will also fluctuate. However, for most laboratory experiments conducted with ice, a constant profile

temperature is applied. The results are then used for extrapolation to more complex situations (Lainey and Tinawi, 1984).

Temperature influences the strength of the ice. Studies show that compressive strength increases with decreasing temperature (Ashton, 2004) as seen in figure 2.5. The tensile strength of ice is almost unaffected by temperature changes.

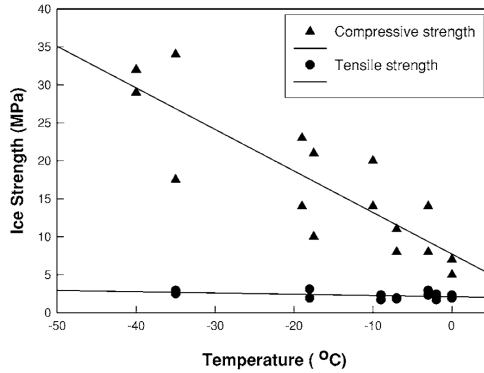


Figure 2.5: Compressive strength and tensile strength of ice versus temperature. From Petrovic (2003)

Strain Rate

The influence of strain rates on ice compressive strength for different temperatures can be seen in figure 2.6. The figure illustrates well how much the compressive strength varies for different ice characteristics. As is illustrated by the two different line styles, the load orientation is also important. The ice can endure higher loads if the load is exerted normal to the growth direction.

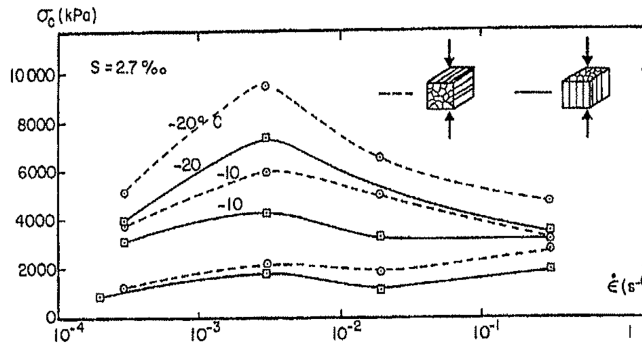


Figure 2.6: Compressive strength versus strain rate. From Marchenko (2013)

Ice Porosity

The porosity, ϕ , is defined as:

$$\phi = \frac{V_v}{V_T} \quad (2.3)$$

Where V_v is the volume of voids and V_T is the total volume. From equation 2.3 it is derived that the porosity of ice can be expressed as:

$$\phi = 1 - \frac{\rho_{ice}}{\rho_i} \quad (2.4)$$

Where ρ_{ice} is the density of ice and ρ_i is the density of pure ice, given in equation 2.1. Schulson and Duval (2009) presents porosity in relation to Young's modulus in figure 2.7. Findings show that for low-porosity ice ($\phi < 10\%$), the Young's modulus decreases for increasing porosity. High porosity results consequently in low ice stiffness. This effect appears to be independent of water content, and is therefore applicable for both saline and freshwater ice, (Schulson and Duval, 2009).

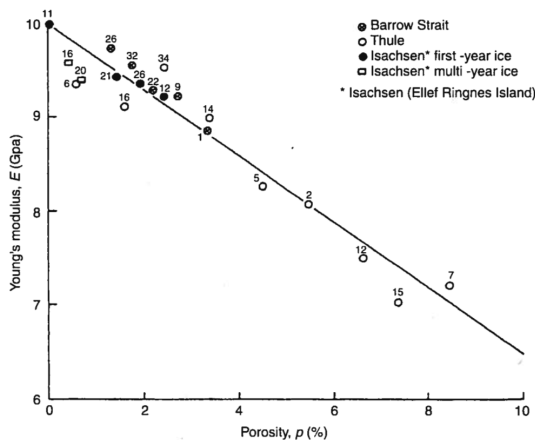


Figure 2.7: Young's modulus vs. porosity of cold, arctic sea ice. From Schulson and Duval (2009)

Orientation

When ice interacts with structures it can fail in several modes. According to Lehmus et al. (1997), part of the ice will be subjected to compression forces. As explained earlier, secondary ice is the predominant ice. By investigating the compressive strength in all three directions of the anisotropic secondary columnar ice, the strength of ice related to orientation could be analyzed.

Lainey and Tinawi (1984) describes the compressive strength of ice in relation to the orientation in figure 2.8. As seen in the figure, depending on the orientation, ice compressive strength varies by a factor of more than 4. Ice is strongest when the load direction is parallel or perpendicular to the column axis. As orientation changes the compressive strength will decrease to a minimum when the c-axis is orientated 45° to the load direction in the horizontal plane.

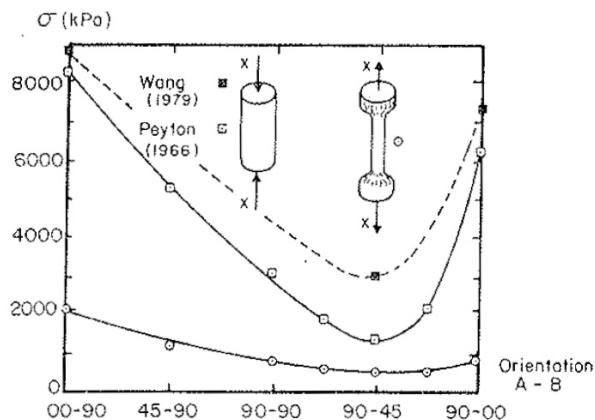


Figure 2.8: Uniaxial compressive strength (■ and □). A refers to the angle between XX and the ice column axis. B refers to the angle between XX and the crystal optic axis (Lainey and Tinawi, 1984)

Lehmus et al. (1997) also presented a comparison of compressive strength of columnar sea ice, for horizontal loading parallel and perpendicular to the c-axis. The study shows similar results as given in figure 2.8. A higher compressive strength for ice horizontally loaded parallel to the c-axis. Results also show a 36% greater strength for vertical loaded ice perpendicular to the c-axis, than for horizontal loaded ice perpendicular to the c-axis. They conclude that the effect is believed to be related to stress concentrations and strengthening effects of the vertically-oriented brine inclusions as seen in figure 2.3. By looking at figure 2.8 and figure 2.2a one can conclude that maximum ice strength (A=00 and B=90, figure 2.8) will not act on a offshore structure. It will depend on the orientation of the c-axis and will most likely be in the area of A = B = 90, which refers to S2 or S3 ice.

Grain Size

The grain size of the ice influences the uniaxial tensile strength and the compressive strength. For fresh water ice, the grain size has been proven to be the key property with regard to development of failure criteria (Cole, 2001). For strain-rates above $4 \times 10^{-6} s^{-1}$ ice strength decrease with increasing grain size. The reverse is observed below that strain-rate, (Cole, 1987).

2.2 Concrete

Concrete in relation to ice-concrete abrasion has been thoroughly described in earlier master thesis where the objective was to investigate concrete ice abrasion resistance, (Kirkhaug, 2013; Bøhn, 2011). As this thesis focuses on the possible effect of ice quality on ice-concrete abrasion and the authors expertise related to ice, theory on concrete will only be presented in short. Outermost relevant concrete theory has been rendered.

2.2.1 Characteristic Strength

As part of the safety philosophy in design codes, concrete is defined by characteristic strength with standard procedures described in the Norwegian code (NS-EN 206-1). For a cylindrical concrete specimen, characteristic cylinder strength, f_{ck} , is defined for a test series of 3 specimens as:

$$f_{ck} \geq f_{cm} - 4 \quad [\text{MPa}] \quad (2.5)$$

Where f_{cm} is the average value of maximum load F , converted to nominal stress for a series of standardized specimens loaded until failure, (Jacobsen et al., 2013).

2.2.2 Effect of Temperature

Concrete volume is affected by temperature changes (ΔT). The magnitude of the thermal dilation (ε_T) is expressed as:

$$\varepsilon_T = \alpha_T \times \Delta T \quad [-] \quad (2.6)$$

Where α_T is the thermal expansion coefficient. Dependent on the type of concrete, α_T may vary somewhat. Different types of aggregates and moisture state affects the coefficient. As a standard, α_T is set to be $10^{-5} \text{ } 1/^\circ\text{C}$, however it can vary in between $5.6 - 13 \cdot 10^{-6} \text{ } 1/^\circ\text{C}$, (Jacobsen et al., 2013).

2.2.3 Profile Roughness

Contact mechanics is greatly related to the interference of materials. The characterization of the surface is thus of interest when investigating the abrading of two interacting materials. Sætre (2013) introduced several methods to characterize the roughness of the concrete samples. Two of the most common parameters will be rendered in this thesis. Namely the average roughness, R_a , and the root mean square roughness, R_q . If we consider points, p_i , along a line with tops and valleys, the average height of these points is \bar{p} . Then R_a is defined as:

$$R_a = \frac{1}{n} \sum_{i=1}^n |\bar{p} - p_i| \quad [\text{mm}] \quad (2.7)$$

And R_q :

$$R_q = \sqrt{\frac{1}{n} \sum_{i=1}^n (\bar{p} - p_i)^2} \quad [\text{mm}] \quad (2.8)$$

2.3 Wear

Structures subjected to ice infested waters will be exposed to drifting ice. As ice encounters these structures, pressure zones builds up and friction forces are induced. These friction forces will cause wear on the susceptible material, (Fosså, 2008). Wear theory and earlier studies on this topic have been described thoroughly in the master thesis of Kirkhaug (2013) and Bøhn (2011). A short review of the abrasion mechanism and supplementary relevant theory will be presented in this section.

2.3.1 Abrasion Mechanism

The ice induced abrasion mechanism on concrete surfaces is of three kinds, see figure 2.9. At the concrete surface, abrasion will occur on a relatively smooth surface. The aggregate stones are covered with cement paste, thus abrasion will at first only occur on the cement. With time, the cement will be abraded and the aggregate stones exposed to the ice. As more cement paste wears off, the bond strength between the aggregates and the cement paste weakens and eventually the aggregates are ripped out, exposing more cement paste. The rate of this mechanism depends on the strength of the cement paste. Studies have shown that aggregates are more ice-abrasion resistant than cement paste (Jacobsen and Scherer, 2013). Ice abrades in a much higher rate than concrete. Dependent on various conditions, wear rate of ice can vary from hundreds to ten thousands of times.

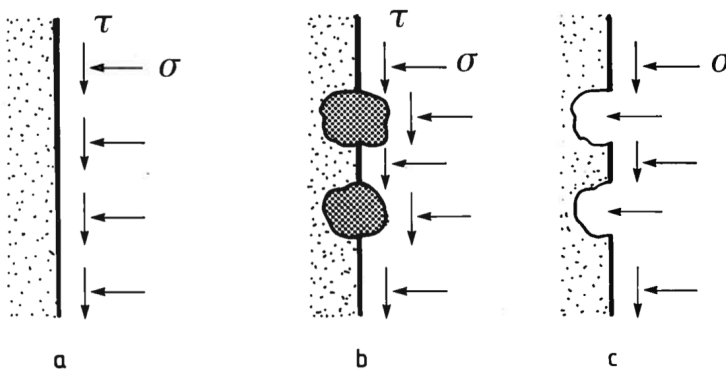


Figure 2.9: Sequence of events in the ice abrasion mechanism. a) Abrasion of cement stone. b) Abrasion of cement paste + loosening of protruding aggregate stone c) abrasion of cement paste when aggregate has loosened. Figure from Huovinen (1990)

2.3.2 Abrasion Variables

Which parameters that influence the abrasion mechanism differ in literature and studies. Jacobsen et al. (2014) states that the majority of the literature at hand is quite empirical and some of it is even contradictory. The absence of a well established theory makes it difficult to identify and monitor all the relevant variables. Numerous estimations on how to model wear rate have been established over the past decades. Kirkhaug (2013) summarized some of the models that have been presented. An improved overview is presented in table 2.1; emphasizing variables affecting the wear mechanism. It is important to address that the findings in table 2.1 are not to be interpreted as absolute. The objective is to display that different researches have estimated the significance of the different variables differently. Note that studies reach apparent opposite conclusions, however this does not indicate that they disagree. Findings can be from different test conditions and magnitudes.

Table 2.1: Summary of reviewed studies on wear variables

Variable	Findings	Study
Contact Pressure	Linear increase in wear vs. contact pressure. Wear depends mainly on it	Itoh et al. (1988)
	Most important factor	Itoh et al. (1994)
	Contact pressure allows for abrasion calculations	Takeuchin et al. (2005)
	Main factor influencing ice abrasion of concrete	Bekker et al. (2012)
	Abrasion depends on contact pressure	Jacobsen et al. (2012)
Sliding Distance	Constant	Hanada et al. (1996)
	Linear relation between mean abrasion and sliding distance	Saeki (2010)
Sliding Velocity	Slight effect on wear rate, but not critical. Affects friction coefficient.	Itoh et al. (1988)
	More important factor than concrete quality governing ice abrasion	Janson (1988)
	No impact	Hanada et al. (1996)
	As the relative velocity increases, the mean abrasion rate decreases	Saeki (2010)
	Abrasion depends on it	Jacobsen et al. (2012)

Continued on next page

Variable	Findings	Study
	Main factor influencing ice abrasion of concrete	Bekker et al. (2012)
Concrete Strength	May have no effect on on wear rate	Itoh et al. (1988)
	Mean abrasion amount and rate is not affected by concrete strength	Saeki (2010)
Aggregate Size	Smaller stone size causes lower abrasion rate	Hanada et al. (1996)
	Wear is especially related to aggregate size	Fiorio (2005)
Compression Strength Stone	Higher strength causes higher ice abrasion resistance	Hanada et al. (1996)
	May have no effect	Itoh et al. (1988)
Concrete Surface	Wet concrete surface has been observed to cause more abrasion than a dry surface	Jacobsen et al. (2012)
Ice Strength	Significant ice strength make abrasion depth critical	Jacobsen et al. (2012)
	Main factor influencing ice abrasion of concrete	Bekker et al. (2012)
	The breaking of the ice is the dominant factor that causes ice abrasion	Janson (1988)
Ice Crystal Hardness	Can be higher than concrete tensile strength. Is a limiting factor.	Jacobsen et al. (2012)
Ice Roughness	Brine pockets result in rough ice surface to increase the abrasion rate	Itoh et al. (1994)
Ice Thickness	More important factor than concrete quality governing ice abrasion	Janson (1988)
Ice Temperature	Lower temperature causes higher wear rate. Wear depends mainly on it.	Itoh et al. (1988)
	Most important factor	Itoh et al. (1994)
	Abrasion affected by temperature	Saeki (2010)
	Main factor influencing ice abrasion of concrete	Bekker et al. (2012)

A mild underlying opinion that the effect the softer ice has on concrete abrasion is negligible was perceived in the beginning of this theses by the author. Some of the studies that have been reviewed did not share this opinion. In their work, Takeuchin et al. (2005) conclud that one needs to consider variation of density, uniaxial compression strength, temperature and salinity of ice in future abrasion

studies. Bekker et al. (2010) twists the focal point and concludes in his work that the intensity of the abrasion depends not only on the parameters of ice but on the properties of concrete as well. Kioka and Takeuchi (2012) substantiate the necessity to investigate the effect of ice quality as they in their studies found that when freshwater ice was used instead of saline ice, the wear rate decreased dramatically on rolled structural steel (SS400).

2.3.3 Abrasion Models

Archard (1953) studied the contact area between two interfering materials. From his studies on sliding wear he concluded that the wear rate is proportional to the load (normal force, edit (Jacobsen and Scherer, 2013)) and independent of the apparent area of contact:

$$W = K \times \frac{P}{3a} \quad [\text{m/m}] \quad (2.9)$$

K is a probability factor assuming that a proportion K of the asperities are in contact. P is the load and a is the radius of the circular area of contact, see Archard (1953). Equation 2.9 is a modification of the mechanical wear equation by Holm (1946). The concept of removal of atoms by Holm had to be rejected due to experimental prove and was replaced with removal of wear particles. Archard (1953) found that material was removed rather in lumps than by atomic layers. Huovinen (1990) introduced an emperical model by mounting a concrete specimen to the bow of an ice breaker and sailing through 40 km of ice. He then developed a relation between the abrasion rate and the compression strength of concrete:

$$b = \frac{3}{f_{c,k}} \times s \quad [\text{mm}] \quad (2.10)$$

Where b is the concrete abrasion rate in mm/km, $f_{c,k}$ is concrete compression strength in MPa and s is length of ice movement in km. Equation 2.10 does not account for any ice properties nor for the ice pressure.

Chapter 3

Experimental Set-up and Procedures

3.1 Ice Samples

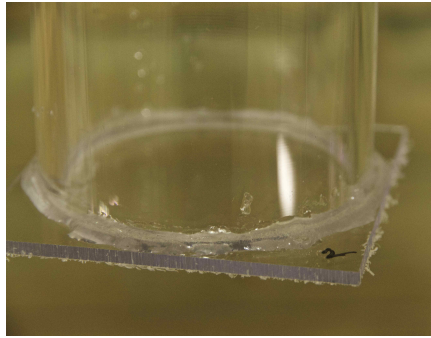
In order to determine the possible effect the ice quality has on ice-concrete abrasion, procedures that yield ice of different qualities have been developed. The experimental set-up conditions have been altered for each of the procedures, knowing how these are effecting ice growth and properties. The focus has been to achieve ice samples with opposing strength and differing texture. The procedure presented in section 3.1.2 was developed to investigate the volumetric change of ice, an aspect highlighted in the pre-study. The time used for freezing, thawing and storage was recorded for all ice samples and is presented in appendix B.

3.1.1 Procedure 1 - Plexiglas Tube

This procedure was developed during the establishment of the project thesis "Ice Quality in Measurements of Concrete Ice Abrasion: Pre-study" and is thoroughly described in section 3.1.2 in (Greaker, 2013). The procedure will be rendered briefly. A plate of plexiglas is fixed to a plexiglas cylinder with an inner diameter of 70 mm by freezing tap water along the outer edges of the tube, see figure 3.1. The tube is filled with cooled tap water and placed in NTNU's cold-lab 1-198 with a room temperature of -10 °C. After minimum 20 hours of freezing, the ice sample is placed in room temperatures and removed from the tube. Subsequently the ice sample is stored in the same cold-lab.



(a) Plexiglas parts. Water squirter used to pour water along the edge in the middle. Figure from Greaker (2013).



(b) Frozen ice along the edges of the plexiglas cylinder holding the parts together.

Figure 3.1: The plexiglas tube

3.1.2 Procedure 2 - POM Tube

POM stands for Polyoxymethylene and is a polymer widely used within engineering due to its good mechanical and chemical properties, (Grigalovica et al., 2013). Because of its creep resistance, high tensile strength and stiffness, tubes were chosen to be made from POM, (Siengchin et al., 2008). Solid cables of POM were purchased from Hatling AS, Trondheim, and processed at NTNU's department of structural engineering. Three tubes with a diameter of 73.5 mm were cut out; 0.1 mm wider than the ice container of the ice abrasion rig. The added 0.1 mm is to compensate for possible shrinkage during solidification of the POM. Additionally a cap of POM was carved to fit perfectly on either side of the tube. This allowed for the tube parts to be put together without any need of adhesives. The POM tube can be seen in figure 3.2.

Tap water from the same sink as in section 3.1.1 was poured into the POM tubes. Thereafter they were placed in the same cold-lab as the samples in procedure 1. After freezing, the tubes were left in room temperatures for thawing. The cap could easily be removed from the tube after some minutes, preventing vacuum forces to be created; see Greaker (2013) for details about vacuum forces. After an average of 25 minutes, the ice sample could be pushed out by hand and be placed back in to the cold-lab for storage.

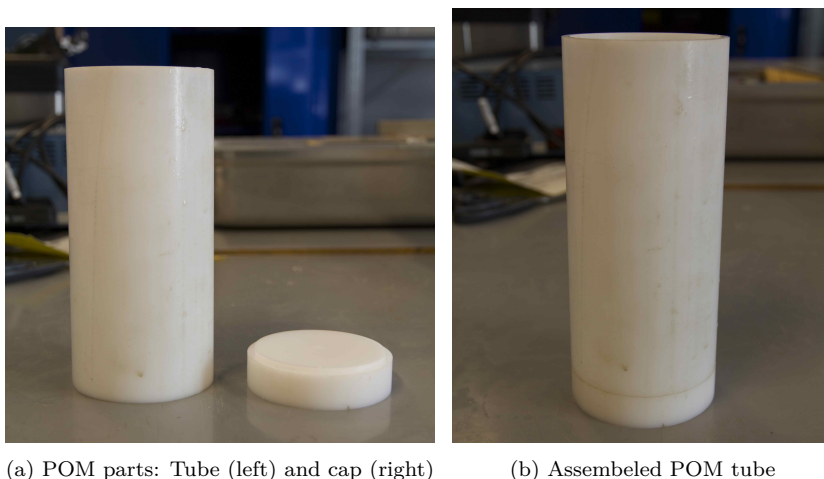


Figure 3.2: The POM tube

3.1.3 Procedure 3 - Agitated Water

The plexiglas parts used in procedure 1 in section 3.1.1 were taken to the cold lab S-109B Frostlab 2, located in room S-119 Utviklingslab at NTNU. The cold-lab was set to have a room temperature of $-20\text{ }^{\circ}\text{C}$. The tube parts were cooled in the cold-lab and assembled by freezing sterilized water along the outer edges of the tube, as described in Greaker (2013). Thereafter the tubes were filled approximately half full with tap water, see figure 3.3a. Several small containers were placed in the cold-lab and filled with a thin layer of tap water. As the water in the containers had frozen, it was pulverized by slamming it with a hammer, creating ice slush seen in figure 3.3b. The water in the tubes were stirred continuously for approximately 3 hours and gradually filled with the ice slush. Once full of slush, they were left in the cold lab-lab to fully freeze, see figure 3.3c.

3.1.4 Procedure 4 - Porous Ice

Plexiglas tubes were assembled as described in procedure 1 and filled with commercial carbonated water. As sparkling water dilates more than tap water, less water should be poured than when using tap water. The top of the tube was sealed with plastic foil in order to diminish gas loss. A glass plate was put on top of that again to add mass and thereby reducing the chance that any pressure build up would break the plastic foil seal. All samples were prepared, frozen and stored in the cold-lab 1-198 with a room temperature of $-10\text{ }^{\circ}\text{C}$. A prepared sample can be seen in figure 3.4a.

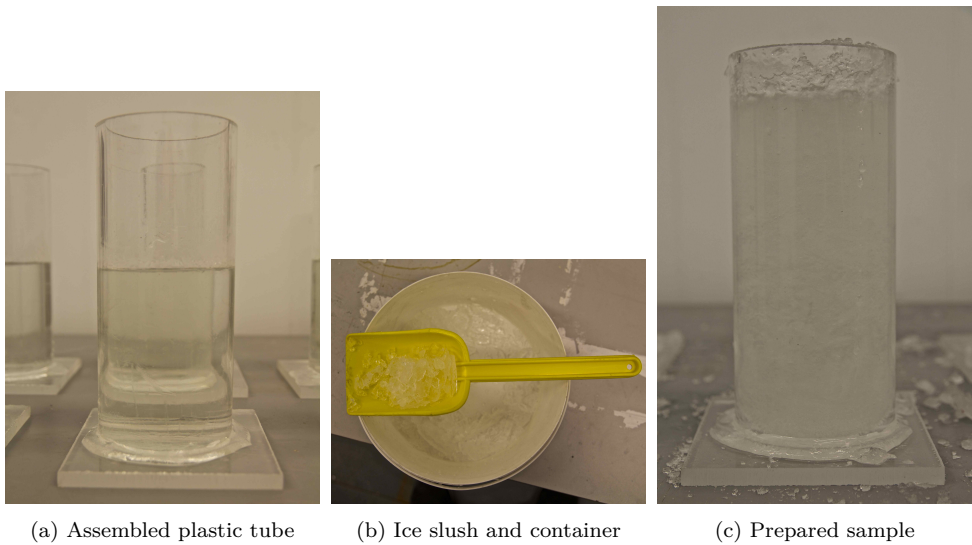


Figure 3.3: Preparation of ice samples with procedure 3

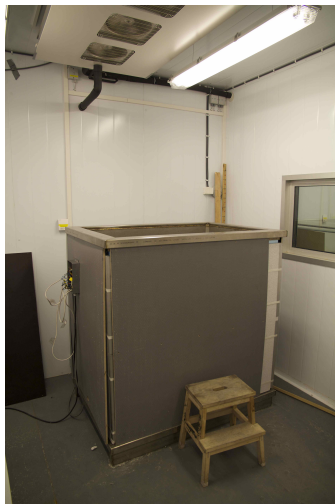


(a) Prepared sample. Glass plate seen on top of the sample, plastic foil wrapped around top part of sample. (b) Close up of figure 3.4a. For scale: Edges of tube seen on either side of the figure. Gas bubbles inside the tube are clearly seen.

Figure 3.4: Preparation of ice samples with procedure 4

3.1.5 Procedure 5 - FRYISIS

FRYSIS is a $120 \times 80 \times 125$ cm custom-made tank located in the S-109B Frostlab 2, see figure 3.5a. The walls of the tank have a heating system installed, which can be regulated by a program made in Labview. The tank was filled with regular tap water and room temperature was set to be -10 °C. In order to reduce unnatural boundary conditions, the walls were set to have a constant temperature of 0 °C. After 7 days, the ice thickness was good for use, measuring 19 cm. A specially designed rack was assembled on top of FRYISIS and a power drill was connected to it. The rack could be moved horizontally and fixed at any desired location on top of FRYISIS. The rack allowed for controlled vertical movement of the drill. Samples were drilled with a hollow core that was attached to the drill. The inner diameter of of the core measured 72 mm. The complete set-up can be seen in figure 3.5b.



(a) FRYISIS



(b) Assembled rack, drill and core

Figure 3.5: Experimental set-up for procedure 5

3.2 Thin Sections

In order to investigate the ice texture of the ice samples made after the different procedures, thin sections were made. The experiment took place in the cold lab S-109B Frostlab 2, located in room S-119 Utviklingslab at NTNU. Ice samples were cut with an Agazzani G. & F.io - Carpi mod:500 n.5261 saw into sections. Horizontal thin sections were cut normal to the length axis of the ice sample and vertical thin sections were cut parallel to the length axis of the sample. Each section was fixed to a 10 ×10 cm glass plate by freezing distilled water along its borders. The samples were placed on a Leitz 1400 microtome and fixed by a vacuum force created by a vacuumbrand membrane-vacuum pump. A Leica 25 cm/c blade was attached to the microtome. The samples were shaved until the surface was free from grime and completely even. Another 10 ×10 cm glass was fixed on the smooth surface and the samples were cut in two. The part with the smooth end was put once more on the microtome and shaved until a remaining thickness of approximately 0.3 mm. Ice crystals will show grey colors under polaroids at a thickness less than 0.2 mm, (Hobbs, 1974). See figure 3.6 for an illustration of a horizontal thin section procedure. The samples were placed under crossed polaroids and inspected in white light on a W. Ludolph. Ice crystals, air pockets and different orientations of the c-axis become recognizable as different colors.

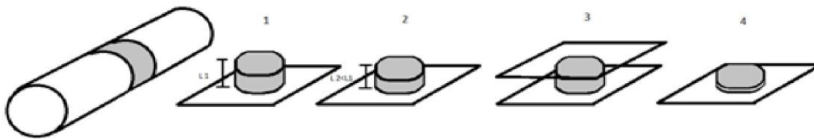


Figure 3.6: Procedure for making a thin section.

3.3 Density and Porosity Measurements

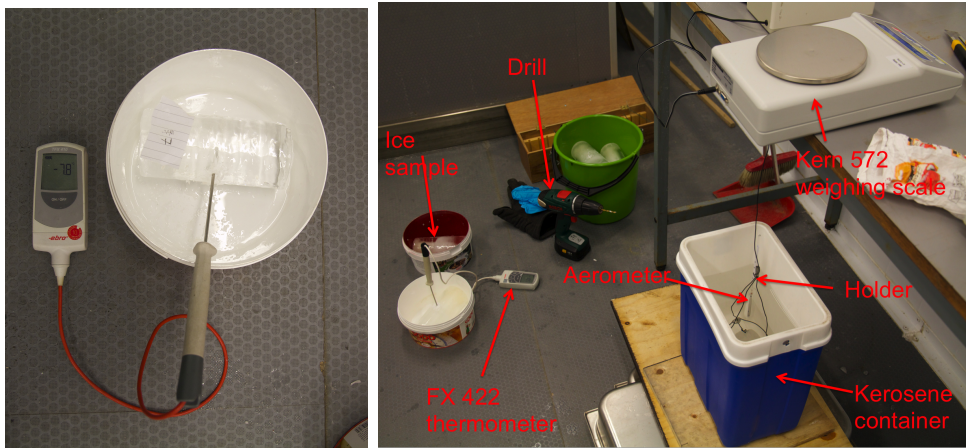
Density and porosity was measured for three ice samples for each procedure. The experimental set-up, see figure 3.7b, was developed during the pre-study to this thesis, (Greker, 2013). In the pre-study it was concluded that this set-up improved the accuracy of the density measurement significantly from earlier thesis. The experimental set-up developed in the pre-study will be briefly summarized in the following. A container was filled with kerosene and cooled down to a temperature below 0 °C. The density of the kerosene was measured continuously with an aerometer and mass was measured with a Kern 572 weighing scale, $d = 0.01$ g. Mass was first measured in air and then submerged in kerosene. The following equation was derived from equation 2.2 to express the ice samples density, ρ_{ice} :

$$\rho_{ice} = \frac{m_{ice+holder,air} - m_{holder,air}}{m_{ice+holder,air} - m_{ice+holder,ker} - \rho_{ker} \times V_{holder}} \times \rho_{ker} \quad (3.1)$$

Where $m_{ice+holder,air}$ is the mass of the ice and the holder. Holder refers to a costume-made container used to enable measurements on objects with smooth surfaces. $m_{holder,air}$ is the mass of the holder, $m_{holder,ker}$ is the mass of the holder submerged into kerosene and ρ_{ker} is the kerosene density. V_{holder} is the volume of the holder which is expressed as:

$$V_{holder} = \frac{m_{holder,air} - m_{holder,ker}}{\rho_{ker}} \quad (3.2)$$

In order to calculate the porosity, temperature was measured. A hole was drilled approximately to the center of the ice sample and temperature was measured with an ebro FX 422 thermometer, see figure 4.25. The pure ice density could then be calculated with equation 2.1. Having calculated the pure ice density, the samples porosity could be determined with equation 2.4.



(a) Temperature recording for sample d7. Temperature was -7.8 °C. (b) Experimental set-up for density and porosity measurements. Figure from Greaker (2013)

Figure 3.7: Experimental set-up for density and porosity measurements.

3.4 Concrete Samples

All ice-concrete abrasion experiments were carried out on concrete of equal quality. The concrete samples used in this report were casted in 2008 and moist cured for approximately 2 years. Since 2010 they were stored in the laboratory at NTNU's department of structural engineering open to air. Samples were casted in 50 mm and 105 mm wide moulds. The batch was an air entrained OPC mortar of $w/c = 0.60$ with 40 volume % paste and 8 mm maximum aggregate size granitic aggregate from Årdal, Norway. This is the same batch as Møen (2009) and Bøhn (2011) used in their master theses.

3.4.1 Sample Preparation

Samples were prepared prior to test conduction in order to minimize unevenness, risk of sample cracking, see page 55 in Bøhn (2011), and to ensure abrasion on concrete samples with an equal fraction of paste and aggregate.

Saw Surface

Samples casted in the 105 mm wide mould were cut in half with a ERRUT saw, see figure 3.8a. Afterwards they were honed on both sides until they were completely even and had a remaining thickness less than 50 mm, see figure 3.8b. Samples with saw surfaces were branded "D", where the two parts originating from the same 105 mm mould are identified 1 and 1.2, for example D1 and D1.2.



(a) Top: Before sawing. Bottom: After sawing. (b) Top: Before honing. Bottom: After honing.

Figure 3.8: Preparation of concrete sample with saw surface.

Casting Surface

As there was not enough samples that had been casted in the 105 mm wide mould, samples casted in the 50 mm wide mould were used in three of the abrasion experiments. These are referred to as casted surface samples and are branded "STD". The samples were honed on both sides with a Seidner grinder. A handle allowed for vertical adjustment of the grinder's blade by 0.4 mm/round. One side of the concrete sample was honed until its entire surface had been in contact with the grinder. The other side, which later would be the side in contact with ice, was honed approximately 2 mm down. A prepared sample can be seen in figure 3.9.



Figure 3.9: Prepared casted surface concrete sample.

3.4.2 Concrete Density

The mass of four concrete samples, both dry and submerged into water, was measured. Density of the concrete samples, ρ_{con} , was thereafter calculated as:

$$\rho_{con} = \frac{m_{con}}{m_{con} - m_{con,s}} \times \rho_w \quad (3.3)$$

Where m_{con} is the mass of the concrete sample, $m_{con,s}$ is the apparent mass of submerged specimen and ρ_w is the density of water at room temperature $\approx 10^3$ kg/m³, (C39, 2014).

3.4.3 Concrete Strength

The compression strength of five concrete cylinders, made from the same batch as the samples used for ice-concrete abrasion, was investigated. The cylinders had dimensions 100×200 mm, which is adequate to the cylinder compression test standard. Compression test was performed with a Toni Technik hydraulic test frame mod. 2031, range 30-3000 kN. Load was applied at 0.5 MPa/s and break sensitivity was set to be 10% . The test-set up can be seen in figure 3.10.

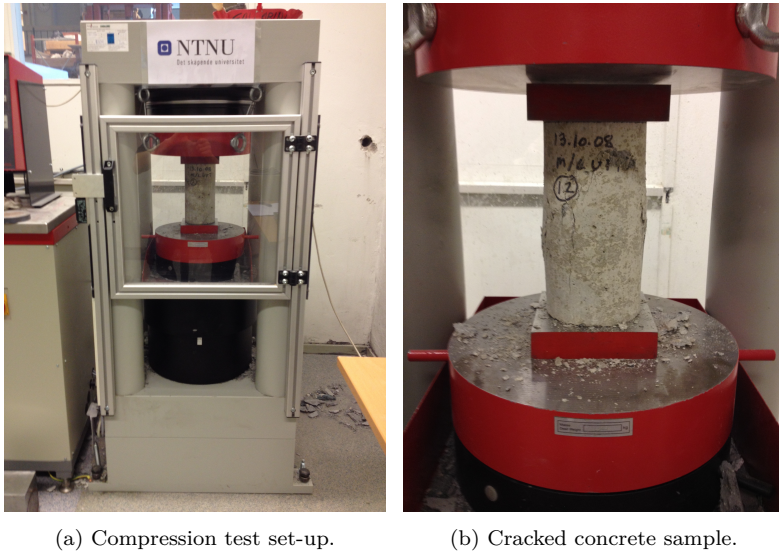


Figure 3.10: Compression test set-up

3.5 Ice-Concrete Abrasion Rig

All abrasion experiments were conducted on the ice-concrete abrasion rig located in the cold-lab 1-198 at NTNU's department of structural engineering, see figure 3.11. All data was recorded by and settings were inputted in the software program Isabrasivmaskin-v3, a program coded in Labview. The abrasion rig was made familiar with in the pre-study to this thesis and was thoroughly described, (Greaker, 2013). Several theses have operated and described the rig, see Kirkhaug (2013); Bøhn (2011); Møen (2009). The abrasion rig is custom built at NTNU for the single purpose of controlled ice-concrete abrasion. Continuous maintenance is necessary to ensure operations. During its service, several modifications have been made to enhance performance. A presentation of the rig and the modifications made for this thesis will be given in the following.



Figure 3.11: Ice-concrete abrasion rig.

According to Hara et al. (1995), the abrasion rig is classified as a sliding contact type. Ice samples are placed in a container connected to a horizontal shaping machine, see figure 3.12a. With a stroke length of 200 mm, the ice sample container travels a total horizontal distance of 400 mm, per cycle. The distance traveled by the container can be chosen to be recorded either per cycle or in Hz in the software Isabrasivmaskin-v3. Experiments in this thesis were chosen to be recorded with maximum frequency, 10 Hz, in order to investigate the variation of the friction coefficient. A motor, seen in blue in figure 3.11, pushes the ice sample towards the underlying concrete sample. This movement is monitored by Isabrasivmaskin-v3, which will automatically stop at a certain remaining ice sample size. The

container can only hold one ice sample, consequently operations has to be stopped in order to change ice samples as they erode. The motor pushes the ice sample in a speed chosen by the operator until a predefined load is reached. The load is automatically maintained and recorded by two load-cells and the feedback system controlled by the software in Labview. The load-cells are located underneath the roller bearings seen in figure 3.12b. On top of the roller bearings is a copper "sandwich" on which the concrete sample rests. The "sandwich", see figure 3.12b, consists of a tube sling casted in epoxy that is enclosed by two copper plates. With success, this construction was designed during the pre-study to compensate for deformations causing sample cracking due to bending moments, see Böhn (2011). The concrete samples were fixed by manually tightening a screw, see left in figure 3.12a. Horizontal load was recorded by a load-cell installed as seen in figure 3.12b.



(a) Piston. Vertical piston attached to the motor and container. Concrete sample on copper "sandwich" underneath container.



(b) Copper "sandwich" to the left and roll bearings are seen to the right of it. Horizontal load-cell further to the right.

Figure 3.12: Details of the ice-concrete abrasion rig. Orange specimen is the ice sample container. Black tubes transports alcohol for temperature regulations in both ice sample container and copper "sandwich".

The room temperature in cold-lab 1-198 is controlled by a Pego 200 Expert control unit. This allows the room temperature to be regulated to temperatures as low as $-20\text{ }^{\circ}\text{C}$ with steps of $0.1\text{ }^{\circ}\text{C}$. Cold air is generated by a fan installed in the labs roof. As there is only one door to the cold-lab, warm air can flow in to the cold-lab whenever the door to the lab is opened. The Julabo 2000 heating circulator seen right

in figure 3.13 allows for temperature regulations in the copper "sandwich" and in the ice sample container. Kirkhaug (2013) found that approximately temperature of 12 °C was needed from the Julabo to obtain a concrete surface temperature of 0 °C, by monitoring the temperature of concrete samples with enclosed thermometers. Room temperature in the cold-lab was recorded during test conduction by a thermochord placed between the rig and the wall closest to the door. The chord was placed close to the engine of the rig which ensures for the horizontal movement of the piston.

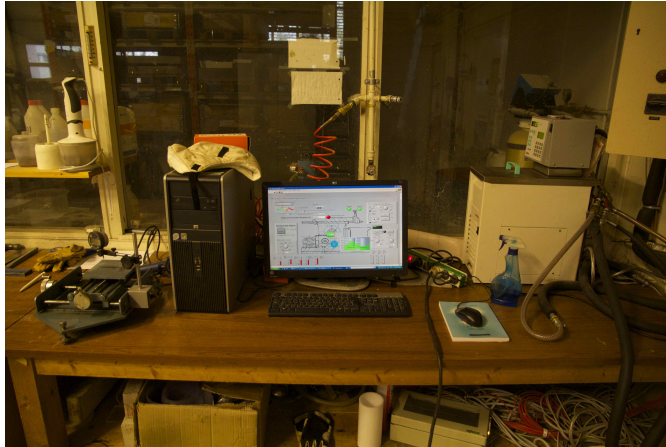


Figure 3.13: Ice-concrete abrasion rig instruments. From left to right: Coordinate-table, Computer running Isabrasivmaskin-v3 and Julabo 2000 heating circulator.

3.5.1 Modifications

There were several challenges with the abrasion rig prior to test conduction. The rig has been completely taken apart and re-assembled. The motor pushing the ice sample has been replaced three times, a bolt holding the piston was replaced and a new and stronger gear box has been installed. The reason was that the desired vertical load could not be reached during trial. Assuming the problem was with the motor, it was replaced. As this did not give any result, a stronger motor was installed, without any success. Later, the problem was found to be that three side panel screws, see figure 3.12a were too tight. Loosening these screws solved the load recording problem.

To change ice samples, the table, on which the concrete sample is placed, has to be moved sideways. The table was earlier moved manually and the concrete sample had to be centered under the ice container by manual adjustments. The motor seen in figure 3.14 was installed so that the table could be moved automatically. Sensors were installed to ensure that the table was equally aligned each time it was moved.



Figure 3.14: Automatically adjustment of table with new motor

It was intended to investigate the possible change of the systems friction coefficient due to a new installed sliding bearing. Experiments would have been performed with equal test conditions as the tests with the old roller bearings logged with the new developed program Isabrasivmaskin-v4. The new program will be able to record data with a frequency of 1000 Hz. The troubleshooting for the low vertical load recording was time-consuming and left no time to investigate the planned abrasion rig set-up.

3.5.2 Test Conditions

Test conditions for all conducted ice-concrete abrasion experiments are shown in table 3.1. Conditions were set to be as alike the conditions used in earlier master thesis, Kirkhaug (2013); Møen (2009), as possible. By having similar test conditions, the results would have a better comparative basis.

Table 3.1: Experimental test conditions for the abrasion rig

Pego 200 Expert:	-10 °C
Vertical load:	4500 N
Sliding velocity:	850 RPM \approx 16 cm/s
Effective sliding distance:	500 m
Julabo 2000 temperature:	11-12 °C
Vertical gain:	0.02 mm
Vertical speed:	600 RPM

3.6 Measurements

3.6.1 Abrasion Depth

The concrete sample surface, which was going to be exposed to ice, was measured with a Mitutoyo Corp. 543-250B ID- C112B digital indicator, $d = 0.003$ mm, (Mitutoyo, 2005). The indicator was connected to a coordinate table, see figure 3.15. Originally, the coordinate table was not made for such large specimens. In order to measure the entire concrete surface, the sample had to be measured in two separate turns. Sætre (2014) developed a measuring procedure that was followed for all measurements. The edge of the concrete sample was aligned with the back edge of the table. Lines were drawn on either side of the sample for each y-axis point. These were meant to make it possible to align the concrete sample equally for each measuring session. One line was aligned with the edge of the table and another one where the measurements were to start (20 mm from the center), see figure 3.15. All samples had starting points (5,-20) and (95,20) calibrated to 0.000 mm. The sample was measured from $y=20$ to $y=100$ first. Thereafter the sample was turned and measured from $y=-20$ to $y=-100$. The measurement had to be performed as such hence the pole connecting the digital indicator and the table otherwise would have crashed with the sample. This is also the reason why no measurements were done at $y=0$.



Figure 3.15: Abrasion depth measurement set-up for initial reference point. From bottom to top: Coordinate table, concrete specimen and digital indicator. Rotation wheels are seen in front and on the left side of the coordinate table.

After ice exposure, the concrete sample was measured again. All surfaces, before and after ice exposure, were measured twice at $11 \times 10 = 110$ predefined grid points, see figure 3.16. The outermost points were placed such that they weren't in contact with ice during abrasion test conduction. These points would not be subjected to ice-concrete abrasion and are referred to as reference points. By maneuvering two wheels, the concrete sample could be moved to each grid point. One wheel rotation equaled 1 mm in either planar direction. Data was noted for every measurement

on a sheet presented in appendix F.

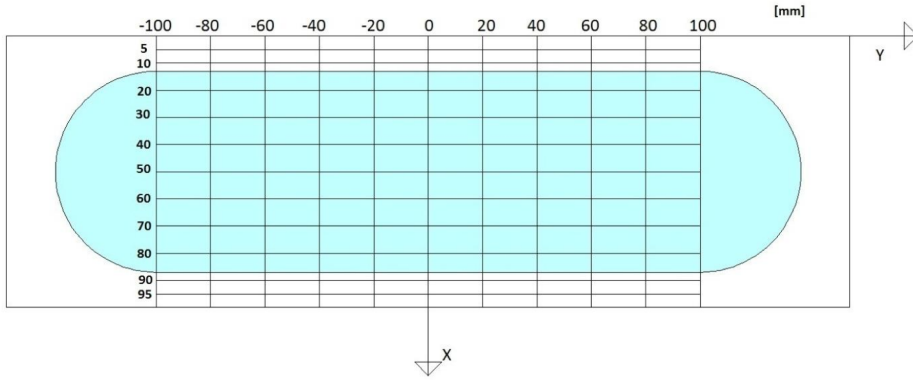


Figure 3.16: Predefined grid points. Area colored blue marks the ice exposed concrete surface. Figure from Kirkhaug (2013)

3.6.2 Abrasion Rate

Measurements were transferred into an Microsoft Excel sheet. The two times 110 measurements before ice exposure and the two times 110 measurements after ice exposure were averaged. Mean and standard deviation, before and after ice exposure, were calculated for the reference points and the exposed points. Two approaches were developed to calculate abrasion depth, namely method 1 and method 2. Where method 1 is an absolute measurement and method 2 is a relative measurement. For both methods, each row was calibrated for the effective ice length due to the circular contact surface between the ice and concrete sample, see section 3.7.2. Abrasion depth was calculated as the average depth of all grid points exposed to ice, and abrasion rate could thereafter be calculated as:

$$\text{Mean abrasion rate} = \frac{\text{Mean abrasion depth}}{\text{Effective sliding distance}} \quad [\text{mm/km}] \quad (3.4)$$

Mean abrasion rate is defined as wear in millimeter per kilometer of ice sliding.

Method 1 - Initial Reference Points

Abrasion depth at each grid point was calculated as the following:

$$\Delta p_{x,y} = p_{x,y} - \hat{p}_{x,y} \quad [\text{mm}] \quad (3.5)$$

Where $p_{x,y}$ is the average grid point height at (x,y) before abrasion, see figure 3.17a, and $\hat{p}_{x,y}$ is the average grid point height at (x,y) after abrasion, see figure 3.17b. Abrasion depth for each grid point, $\Delta p_{x,y}$, is the difference between these two points.

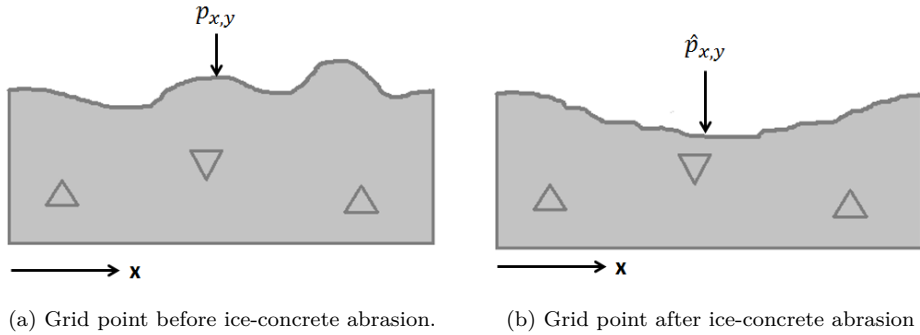


Figure 3.17: Calculation of abrasion rate with method 1. Grid point before abrasion, $p_{x,y}$, and grid point after abrasion, $\hat{p}_{x,y}$.

Method 2 - Outermost Reference Points

Sætre (2014) developed a procedure where each grid point at column y_i are referred to their nearest reference point. The allocation of the grid points is illustrated in figure 3.18a. Blue zone (rows $x=20$ to $x=50$) is referred to reference points at row $x = 5$, while the red zone (rows $x=60$ to $x=80$) is referred to the reference points at row $x=95$. Reference points along $x=10$ and $x=90$ were not used, as it was uncertain whether they during test conduction were in contact with ice or not. The idea is that by referring grid points to their nearest reference point, any systematic error in the measurement set-up would be compensated for. The relative height becomes:

$$\begin{aligned} dp_{x,y} &= p_{ref,y} - p_{x,y} \quad [\text{mm}] \\ d\hat{p}_{x,y} &= \hat{p}_{ref,y} - \hat{p}_{x,y} \quad [\text{mm}] \end{aligned} \quad (3.6)$$

Where $p_{ref,y}$ is the reference point height at $(5,y)$ or $(95,y)$ before abrasion and $p_{x,y}$ is the grid point height before abrasion. $dp_{x,y}$ is the difference between these two points as is illustrated in figure 3.18b. \hat{p} indicates that the sample has been abraded. The abrasion depth can thereafter be calculated as:

$$\Delta p_{x,y} = dp_{x,y} - d\hat{p}_{x,y} \quad [\text{mm}] \quad (3.7)$$

Where $\Delta p_{x,y}$ is abrasion depth at point (x,y) .

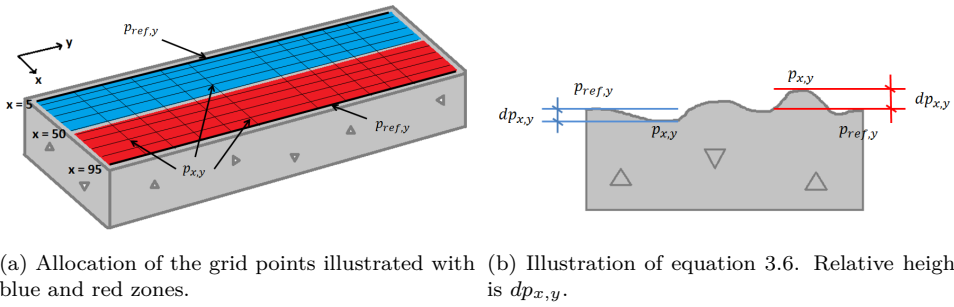


Figure 3.18: Calculation of abrasion rate with method 2. Reference points, $p_{ref,y}$, and grid points, $p_{x,y}$.

3.6.3 Presentation of Conducted Abrasion Experiment

The friction, load and air temperature in the cold-lab was recorded for all experiments by Isabrasivmaskin-v3. This data was processed with the computing software MATLAB® by MathWorks®. The script which was used to graphically present the recorded data is attached in appendix H. It is hoped that forthcoming experiments can be evaluated with this script and thereby simplify experimental comparison. Instructions on how to run the script are found at the beginning of the script.

3.7 Calibrations

3.7.1 Effective Sliding Distance

The program Isabrasivmaskin-v3 records the accumulated sliding distance of the ice sample. To determine the effective ice sliding distance to which the concrete sample is exposed to the sliding distance has to be calibrated. The effective ice sliding distance can be found by multiplying the accumulated sliding distance with the correction factor:

$$\text{Correction factor} = \frac{D}{l} = \frac{73.4 \text{ mm}}{200 \text{ mm}} = 0.367 \quad [-] \quad (3.8)$$

Where D is the ice sample container diameter and l is the stroke length.

$$\text{Eff. sliding distance} = \text{Acc. sliding distance} \times \text{Cor. factor} \quad [\text{km}] \quad (3.9)$$

According to equation 3.9, one kilometer of ice sliding equals $1 \text{ km} \times 0.367 = 367 \text{ m}$ of ice exposure on the concrete sample. In earlier reports the correction factor used was 0.37, (Møen, 2009; Bøhn, 2011; Kirkhaug, 2013; Greaker, 2013). The reason for this was that the diameter of the ice sample container was set to be 74 mm. A more precise measurement showed that the correct container diameter was 73.4 mm. In order to compare results from this report to earlier reports, effective sliding distance has been calculated with a correction factor of 0.37.

3.7.2 Chord Calibration

Due to the circular contact surface of the ice sample, equation 3.9 applies only at the center of the ice sample. Concrete exposed off center will experience less ice movement. Kirkhaug (2013) describes how this can be accounted for in section 3.7 and the calibration factors can be found in table 11, (Kirkhaug, 2013).

3.7.3 Thermal Expansion

Tested concrete specimens are subjected to different thermal regimes. According to section 2.2.2, this will inflict the abrasion measurements as the following:

$$\varepsilon_T = 10^{-5} \text{ 1/}^\circ\text{C} \times (20 \text{ }^\circ\text{C} - 6 \text{ }^\circ\text{C}) = 1.4 \cdot 10^{-4}$$

$$\Delta L = 1.4 \cdot 10^{-4} \times 50 \text{ mm} = 0.007 \text{ mm}$$

Where ε_T is the thermal strain and ΔL is the change in length. When the concrete sample is taken from the cold-lab into room temperature, it can be assumed an average sample temperature of 6 °C and a room temperature of 20 °C. This would mean that the concrete sample could theoretically dilate up to 0.007 mm in all directions. In order to reduce thermal interference on abrasion measurements, see section 2.2.2, concrete samples were stored in room temperature for a minimum of three days after test conduction.

3.8 Analysis of earlier Ice Abrasion Results

Abrasion results presented in master thesis of Kirkhaug (2013) and Møen (2009) have been compared and analyzed. Results retrieved from Kirkhaug (2013) consists of abrasion rate measurements taken on two parallel samples. Abrasion rate was recorded twice for each sample after 1250 meters and after 2500 meters of effective ice sliding. Møen (2009) performed only tests on the same concrete as used in this thesis. Møen had only an effective sliding distance of 185 meters and abrasion was recorded at the end of trial. The results were collected in a spreadsheet and the mean abrasion rate and standard deviation were calculated for each concrete type and test condition, see appendix E. Mean abrasion rate was calculated according to equation 3.4. In addition, the relative difference in abrasion rate between two parallel concrete samples was calculated as:

$$\text{Relative difference} = \frac{|\text{Abrasion rate}_{S1} - \text{Abrasion rate}_{S2}|}{\text{Mean abrasion rate}} \quad [-] \quad (3.10)$$

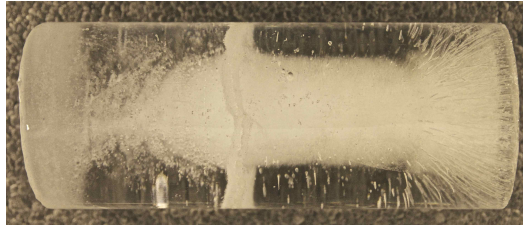
All data was processed with the computing software MATLAB® by MathWorks®.

Chapter 4

Results

4.1 Ice Samples

Ice samples made after the various procedures introduced in section 3.1 are presented in figure 4.1. The diameter, d , of the sample is given respectively in each figure and sample length, l , varied in the range $160 < l < 190$ mm. In figure 4.1 one can clearly see how the ice samples made after the various procedures differ visually. Ice samples from procedure 1 and 2, respectively in figures 4.1a and 4.1b, have the same appearance as the ice samples that were made in the pre-study, (Greaker, 2013). Both ice samples from procedure 3 and 4 are turbid in appearance, procedure 3 having a more murky white color than procedure 4. Tho it is not visible in figure 4.1c, the ice samples made after procedure 3 had a thin layer of clear ice along the edges of the sample. This layer resembles the thicker layer of clear ice seen for both procedure 1 and 2. It is a bit hard to detect, in figure 4.1d there are cavities of different sizes scattered over the samples of procedure 4. As they were removed from their cylinders, one could hear how gas was expelled from these pockets. Procedure 5 made ice almost completely transparent with no concentration of air. Due to the vibrations of the covax during drilling, sample surface had a wavy pattern.



(a) Ice sample made after procedure 1. $d = 70$ mm



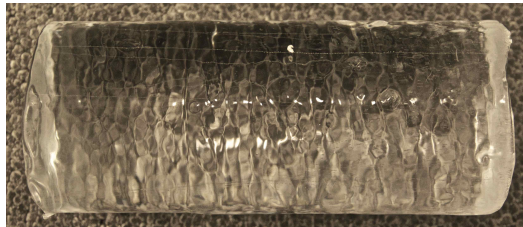
(b) Ice sample made after procedure 2. $d = 73.4$ mm



(c) Ice sample made after procedure 3. $d = 70$ mm



(d) Ice sample made after procedure 4. $d = 70$ mm



(e) Ice sample made after procedure 5. $d \approx 72$ mm

Figure 4.1: Ice samples made after the different procedures presented in section 3.1. Top of the ice sample to the left. Diameter, d , is given for each procedure.

4.2 Thin Sections

Thin sections were made from three ice samples for each of the five procedure presented in section 3.1. For each ice sample, thin sections were taken at the top, bottom and center of the sample. Results can be seen in figure 4.2 to figure 4.16 . The top and bottom sections are horizontal, normal to to the length axis, whereas the center section is vertical, parallel to the length axis of the sample. Vertical thin sections are presented such that the bottom of the figure is towards the bottom of the ice sample. Persistent for all procedures is that the thin sections, within each procedure, resemble each other.

4.2.1 Thin Sections of Procedure 1 - Plexiglas Tube

Diameter of horizontal section is 70 mm. Vertical section is $\approx 90 \times 70$ mm. Horizontal sections show grains stretching towards sample center. Vertical sections with horizontal grain orientation at the edges and curving towards center with vertical growth direction at center. Large black spots, as seen in figures 4.2b, 4.2c and 4.3b, are due to the absence of ice.

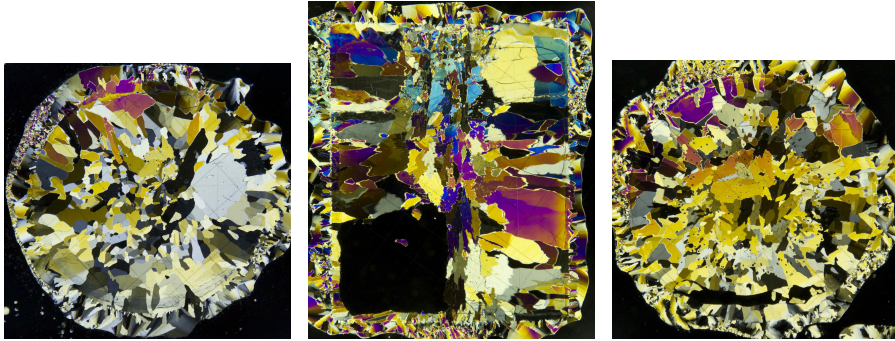


(a) Horizontal section at the top.

(b) Vertical section at the center.

(c) Horizontal section at the bottom.

Figure 4.2: Thin section of sample 14 made after procedure 1.



(a) Horizontal section at the top. (b) Vertical section at the center. (c) Horizontal section at the bottom.

Figure 4.3: Thin section of sample15 made after method 1.



(a) Horizontal section at the top. (b) Vertical section at the center. (c) Horizontal section at the bottom.

Figure 4.4: Thin section of sample 16 made after procedure 1.

4.2.2 Thin Sections of Procedure 2 - POM Tube

Diameter of horizontal section is 73.4 mm. Vertical section is $\approx 90 \times 73.4$ mm. Resembling the top horizontal sections in the pre-study, horizontal section in figure 4.5a shows grain sizes $\approx 1 \times 4$ cm and growth towards sample center. In the vertical sections, large grains at the edges and vertical grain growth direction at center can be seen.

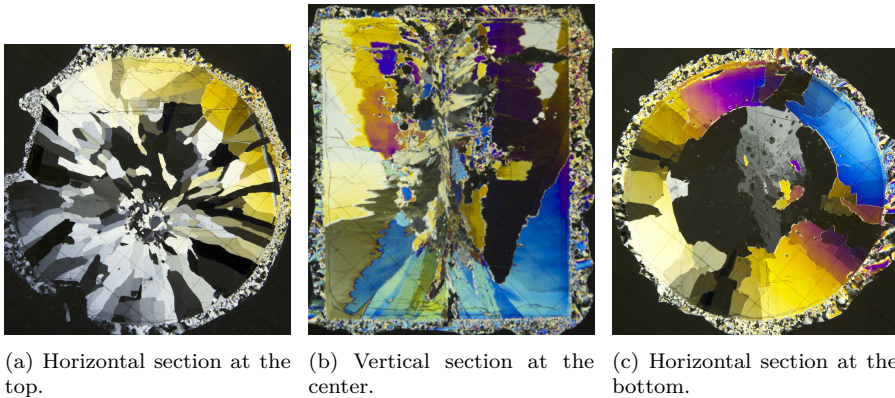


Figure 4.5: Thin section of sample a24 made after procedure 2.

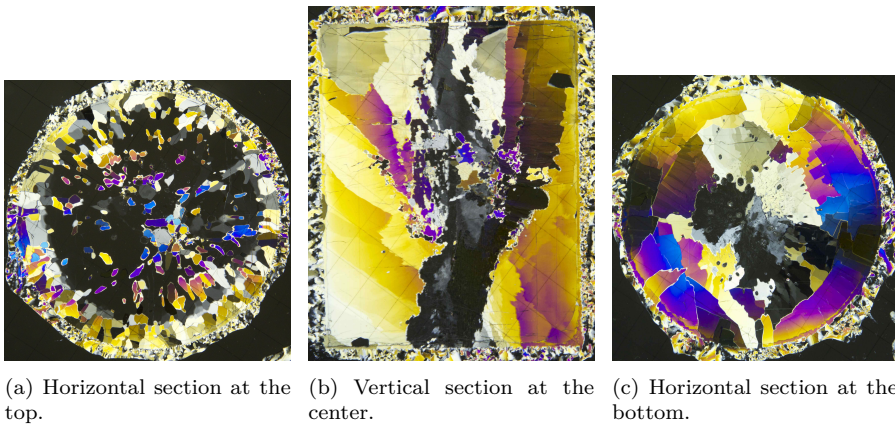
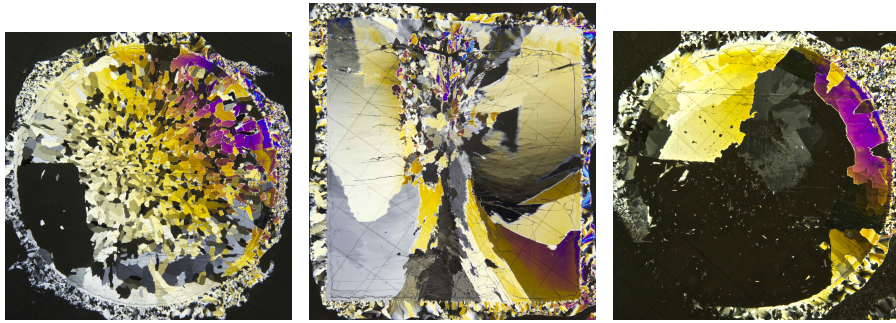


Figure 4.6: Thin section of sample a25 made after procedure 2.

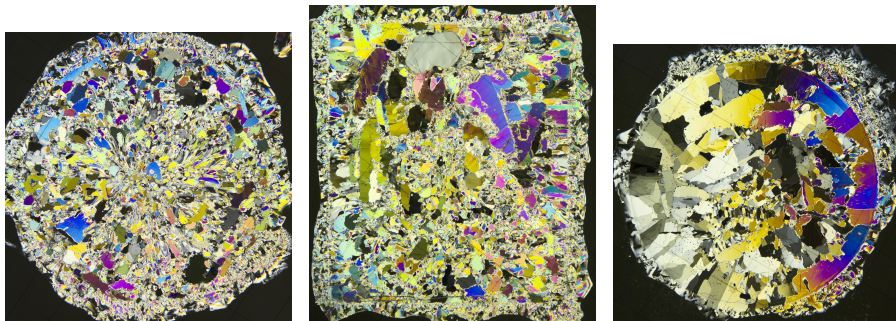


(a) Horizontal section at the top. (b) Vertical section at the center. (c) Horizontal section at the bottom.

Figure 4.7: Thin section of sample a26 made after procedure 2.

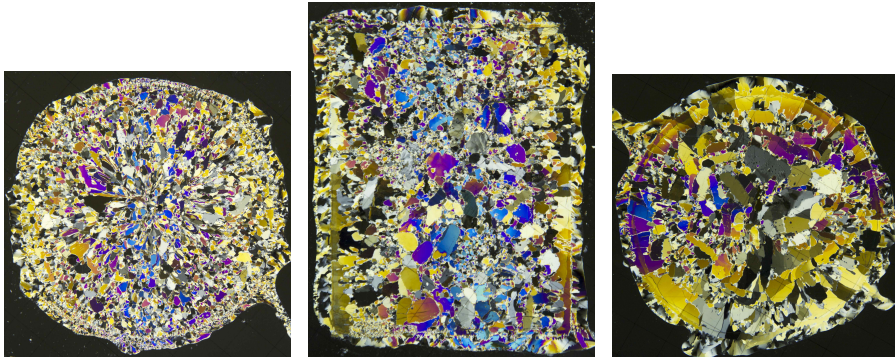
4.2.3 Thin Sections of Procedure 3 - Agitated Water

Diameter of horizontal section is 70 mm. Vertical section is $\approx 90 \times 70$ mm. Small grains are seen in the top horizontal sections and vertical sections. This is a result of rapid crystal growth caused by the low temperature and the mixing of slush and water. Larger grains can be observed in the bottom sections, and is due to the floating of ice slush. This indicates a slower freezing of the bottom section, and is cohesive with ice theory, see Greager (2013).



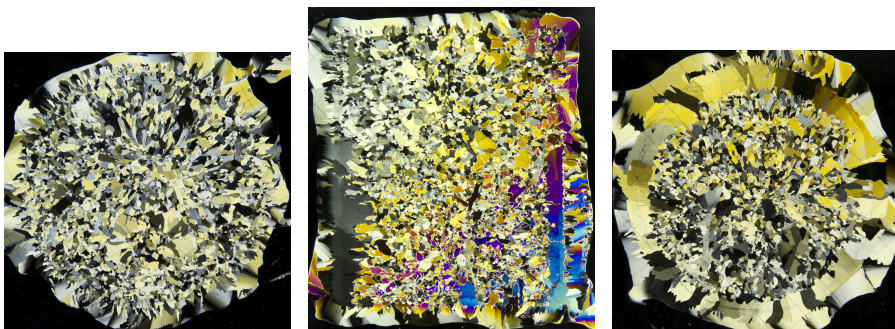
(a) Horizontal section at the top. (b) Vertical section at the center. (c) Horizontal section at the bottom.

Figure 4.8: Thin section of sample b7 made after procedure 3.



(a) Horizontal section at the top. (b) Vertical section at the center. (c) Horizontal section at the bottom.

Figure 4.9: Thin section of sample b8 made after method 3.



(a) Horizontal section at the top. (b) Vertical section at the center. (c) Horizontal section at the bottom.

Figure 4.10: Thin section of sample b11 made after procedure 3.

4.2.4 Thin Sections of Procedure 4 -Porous Ice

Diameter of horizontal section is 70 mm. Vertical section is $\approx 90 \times 70$ mm. A large number of gas pockets can be seen in the thin sections as small black spots. Apart from the gas pockets, ice texture resembles that of p1 and p2.

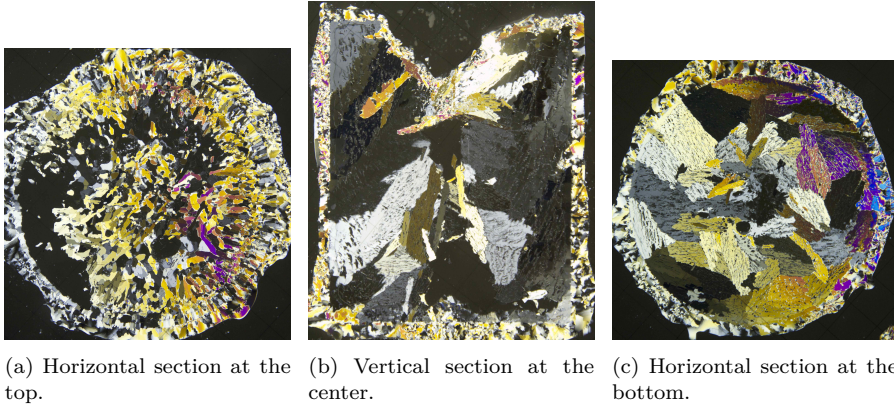


Figure 4.11: Thin section of sample c12 made after procedure 4.

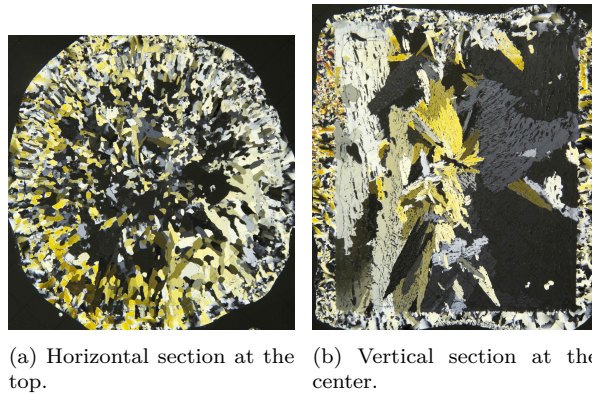


Figure 4.12: Thin section of sample c13 made after procedure 4.

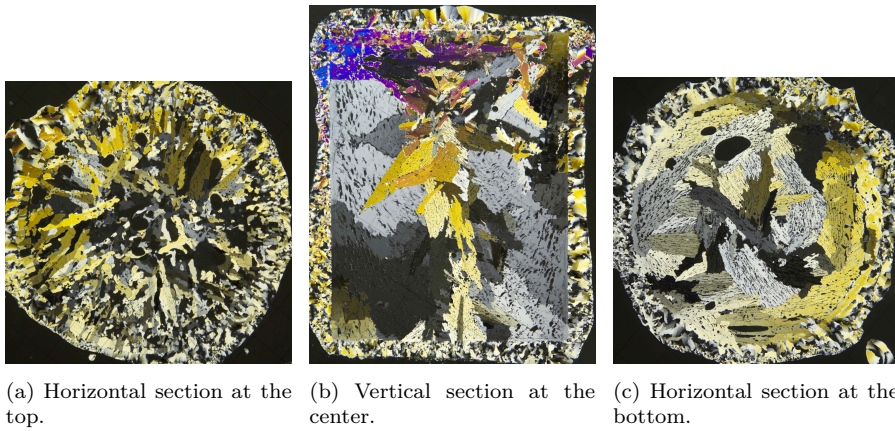


Figure 4.13: Thin section of sample c14 made after procedure 4.

4.2.5 Thin Sections of Procedure 5 - FRY SIS

Diameter of horizontal section is 70 mm. Vertical section is $\approx 90 \times 70$ mm. Sections are showing large grains and horizontal growth direction.

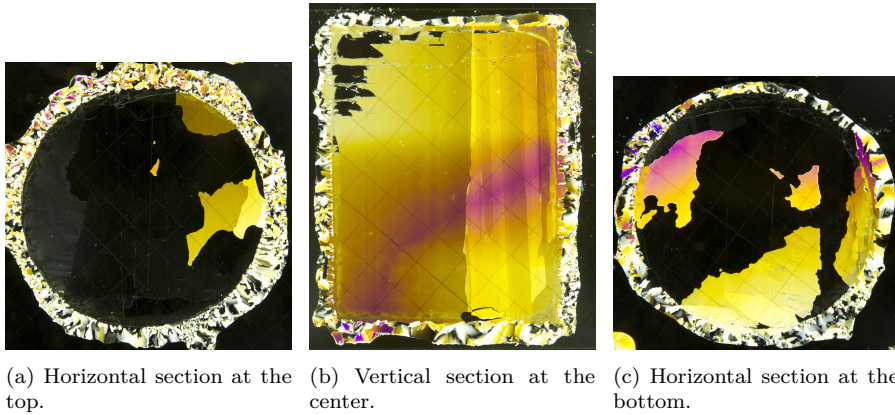
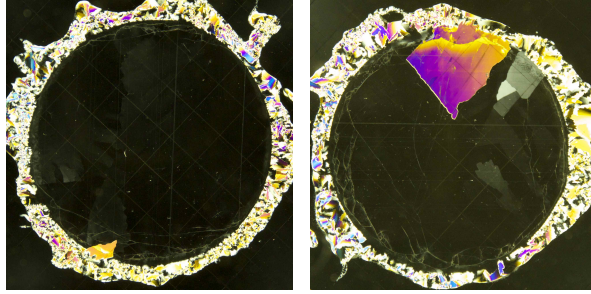
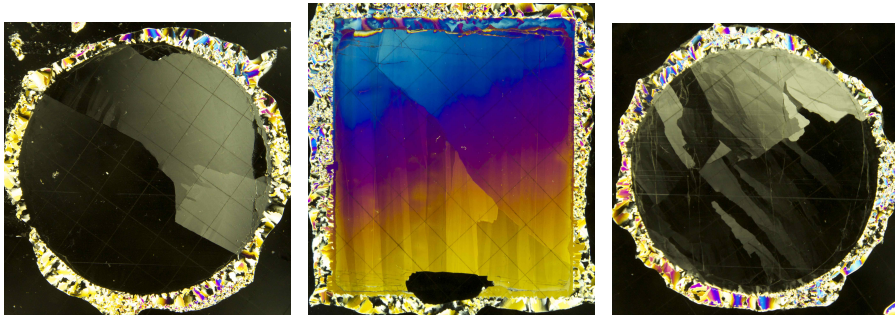


Figure 4.14: Thin section of sample d5 made after procedure 5.



(a) Horizontal section at the top. (b) Horizontal section at the bottom.

Figure 4.15: Thin section of sample d9 made after procedure 5.



(a) Horizontal section at the top. (b) Vertical section at the center. (c) Horizontal section at the bottom.

Figure 4.16: Thin section of sample d22 made after procedure 5.

4.3 Ice Density and Porosity

The densities and porosities calculated from the recorded data shown in appendix C are presented in table 4.1. Greatest difference was measured between procedure 4 and procedure 5. Lowest density and thereby the greatest porosity was measured for procedure 4, $\rho_{ice} = 772.8 \pm 16.2 \text{ kg/m}^3$. The greatest density and thereby the lowest porosity was measured for procedure 5, $\rho_{ice} = 909.8 \pm 0.3 \text{ kg/m}^3$. The densities of procedure 1, 2 and 3 were measured to be approximately the same.

Table 4.1: Results for ice sample density, ρ_{ice} , and porosity, ϕ , measurements.

Procedure	Ice sample	$\rho_{ice} \text{ [kg/m}^3]$	$\phi[\%]$
1	17	901.3	1.8
	18	900.6	1.9
	19	903.1	1.6
2	a27	901.1	1.9
	a28	900.4	1.9
	a29	899.8	2.0
3	b12	898.4	2.1
	b13	898.5	2.0
	b14	898.4	2.1
4	c15	791.5	13.8
	c16	766.0	16.6
	c17	761.4	17.0
5	d7	909.5	0.9
	d11	909.9	0.9
	d21	910.1	0.9
Mean, μ , and standard deviation, σ			
Procedure 1	$\rho_{ice} = 901.7 \pm 1.3$	[kg/m ³]	
Procedure 2	$\rho_{ice} = 900.4 \pm 0.6$	[kg/m ³]	
Procedure 3	$\rho_{ice} = 898.4 \pm 0.1$	[kg/m ³]	
Procedure 4	$\rho_{ice} = 772.8 \pm 16.2$	[kg/m ³]	
Procedure 5	$\rho_{ice} = 909.8 \pm 0.3$	[kg/m ³]	

4.4 Concrete Strength and Density

Mean compression strength, f_{cm} , for the concrete batch used in the conducted ice-concrete abrasion experiments was calculated to be 50.7 ± 0.7 MPa. The density of the same concrete, ρ_{con} , was calculated to be 2249 ± 10 kg/m³. The result for each of the five conducted compression tests is presented in table 4.2, while results of the density measurement are presented in appendix D.

Table 4.2: Concrete strength and the corresponding density, ρ_{con}

Strength, f_c [MPa]	Density, ρ_{con} [kg/m ³]
51.3	2256
51.5	2258
50.1	2235
50.3	2248
50.3	-

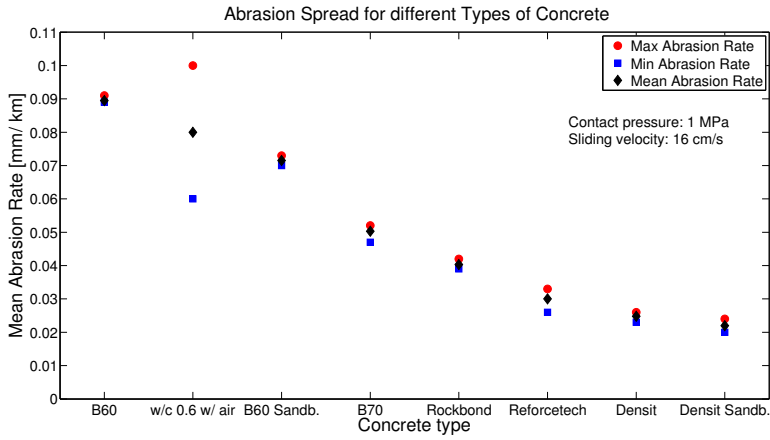
According to equation 2.5 the average characteristic cylinder strength, f_{ck} , for the five concrete samples tested is 46.7 MPa. From table 12.1, (Jacobsen et al., 2013), the concrete class of the tested samples is thereby B45.

4.5 Analysis of earlier Ice Abrasion Results

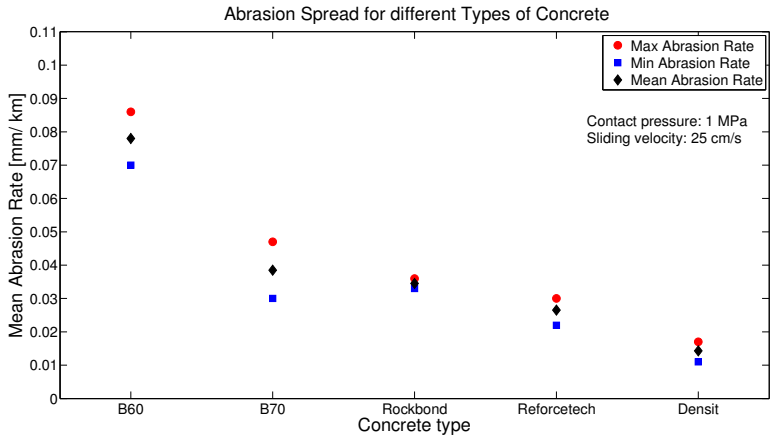
The abrasion data collected from earlier thesis has been computed with MATLAB® and is presented in the following.

4.5.1 Abrasion Rate vs. Concrete Type

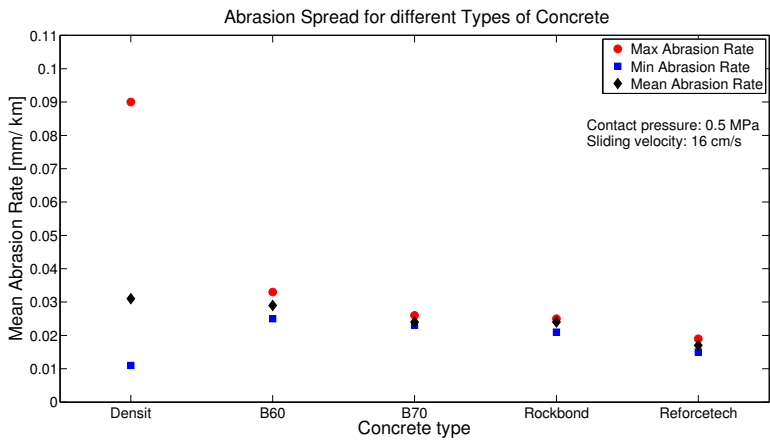
Mean abrasion rates for various concrete specimens are sorted from high to low in figure 4.17. Results are presented for three combinations of the test conditions; contact pressure and sliding velocity. Room temperature during the experiments was -10 °C. Additional test conditions can be found in the master thesis of Kirkhaug (2013). High mean abrasion rates emphasizes concrete with poor ice abrasion resistance, where low abrasion rates emphasize more ice abrasion resistant concrete. For each concrete type, maximum and minimum rates are plotted as red and blue dots respectively.



(a) Sliding velocity 16 cm/s and 1 MPa average contact pressure.



(b) Sliding velocity 25 cm/s and 1 MPa average contact pressure.

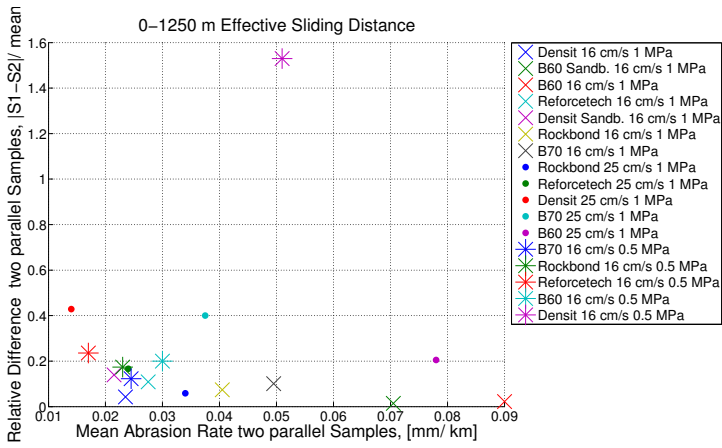


(c) Sliding velocity 16 cm/s and 0.5 MPa average contact pressure.

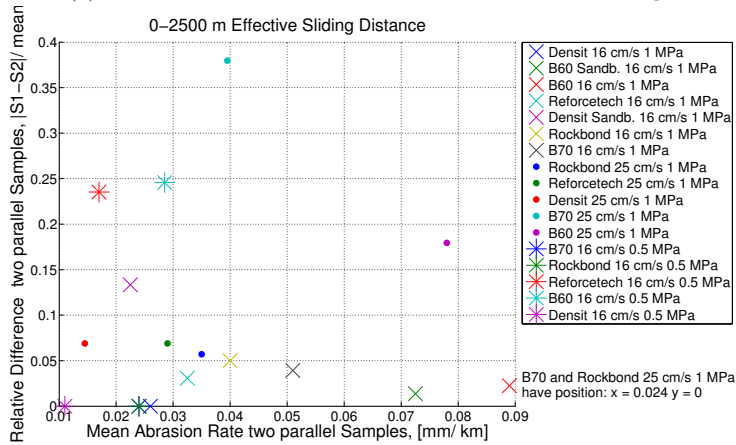
Figure 4.17: Abrasion rate vs. concrete types.

4.5.2 Abrasion Rate vs. Relative Difference

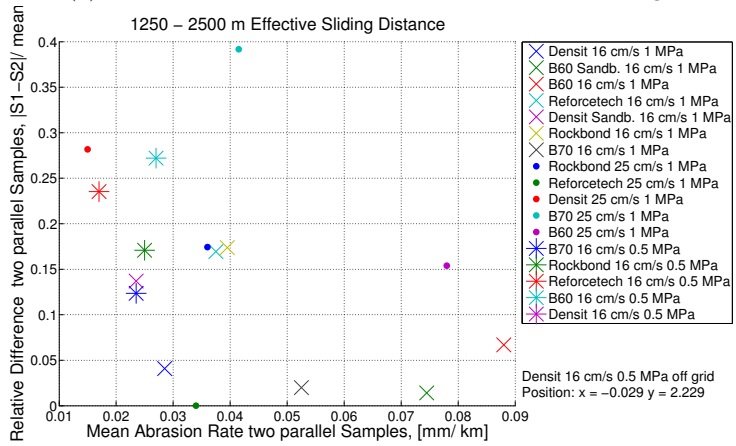
The relative difference between two parallel samples found from equation 3.10 is plotted against the corresponding mean abrasion rate in figure 4.18. Results are presented after 1250 meters, figure 4.18a, from 1250 to 2500 meters, figure 4.18c, and after 2500 meters, figure 4.18b, of effective ice sliding. Each combination of concrete type, sliding velocity and contact pressure has a specific color and marker composition as presented in the legend. Figure 4.18b only shows 16 plots as both B70 concrete and Rockbond concrete with test conditions 16 cm/s sliding velocity and 0.5 MPa average contact pressure have the same values and are therefore overlapping each-other.



(a) Abrasion rate vs. relative difference after 1250 m sliding distance.



(b) Abrasion rate vs. relative difference after 2500 m sliding distance.



(c) Abrasion rate vs. relative difference from 1250 to 2500 m sliding distance.

Figure 4.18: Relative difference vs. abrasion rate.

4.6 Abrasion Rig

Results from a total of 15 ice-concrete abrasion tests are presented in the following. An overview of the conducted abrasion tests and ice samples used is presented in appendix G.

4.6.1 Abrasion Rate

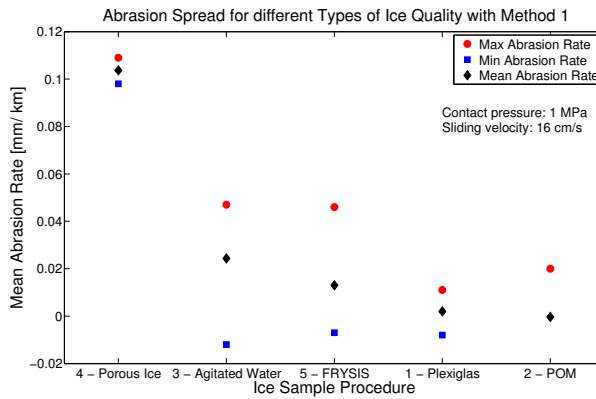
Each of the five ice procedures introduced in section 3.1 were tested on three concrete samples of apparent equal quality. The mean abrasion rate \pm standard deviation was calculated with method 1 and 2, which are described in section 3.6.2. The results from the 15 conducted experiments are presented in table 4.3.

Table 4.3: Abrasion rate \pm standard deviation for the the five different ice sample procedures. Positive number signifies abrasion on concrete sample.

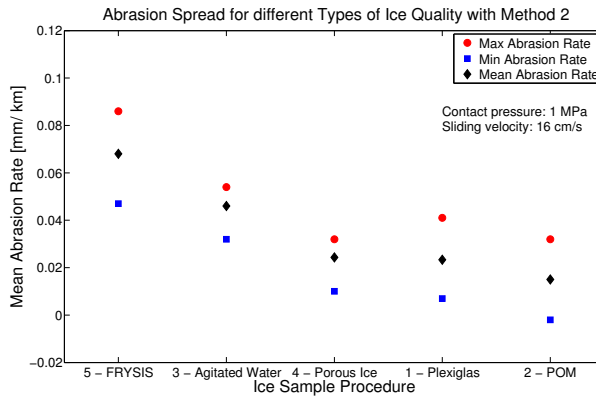
Procedure	Concrete Sample	Abrasion rate [mm/km]	
		Method 1	Method 2
1	STD9	0.011 ± 0.046	0.041 ± 0.043
	STD12	0.003 ± 0.051	0.022 ± 0.041
	STD6	-0.008 ± 0.029	0.007 ± 0.065
2	D8.2	0.008 ± 0.025	0.032 ± 0.035
	D4	0.020 ± 0.147	0.015 ± 0.170
	D1	-0.029 ± 0.298	-0.002 ± 0.302
3	D2	0.047 ± 0.085	0.054 ± 0.089
	D8	0.038 ± 0.057	0.052 ± 0.040
	D2.2	-0.012 ± 0.041	0.032 ± 0.058
4	D7	0.109 ± 0.088	0.031 ± 0.068
	D7.2	0.104 ± 0.073	0.010 ± 0.041
	D6.2	0.098 ± 0.065	0.047 ± 0.051
5	D6	0.046 ± 0.073	0.086 ± 0.086
	D1.2	0.000 ± 0.123	0.071 ± 0.099
	D4.2	-0.007 ± 0.051	0.046 ± 0.036

4.6.2 Abrasion Rate vs. Ice Quality

Results from table 4.3 are presented as mean abrasion rate vs. ice procedure in figure 4.19. Figure 4.19a shows results calculated with method 1, while figure 4.19b shows results after calculation method 2. Both figures are showing mean abrasion rate, maximum abrasion rate and minimum abrasion rate for each ice making procedure. Ice procedure to the left in the figure have the highest calculated abrasion rate, which descends from left to right. Positive value indicates abrasion, while a negative abrasion rate would indicate material buildup and is interpreted as an error. Measurement errors will be discussed in section 5.3. To simplify comparison, the mean abrasion rate for both calculation methods are shown together in figure 4.20a. The correlation between the calculation methods is shown in figure 4.20b.

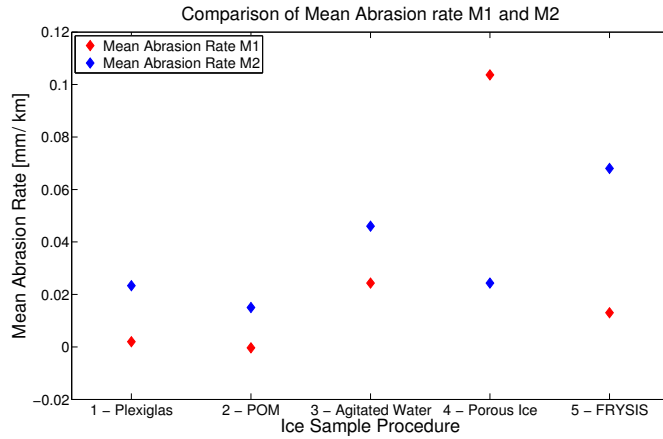


(a) Abrasion rate vs. ice quality with calculation method 1.

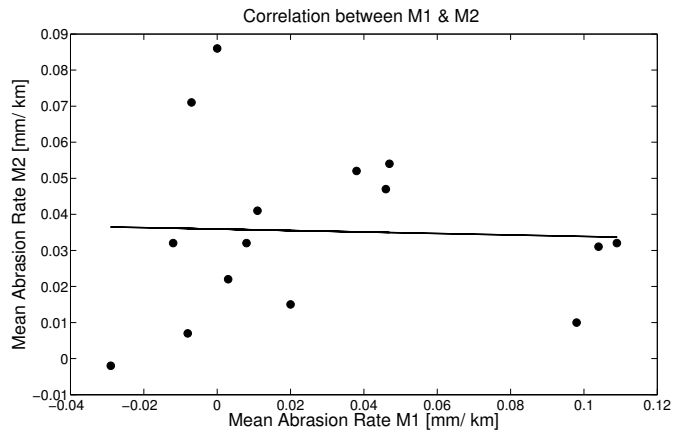


(b) Abrasion rate vs. ice quality with calculation method 2.

Figure 4.19: Abrasion rate vs. ice quality. Positive value indicates abrasion.



(a) Comparison of mean abrasion rate with calculation method 1 and 2.



(b) Correlation between calculation method 1 and 2.

Figure 4.20: Comparison of the two calculation methods. Positive value indicates abrasion.

4.6.3 Profile Roughness

The surface roughness, R_a , and mean square roughness, R_q have been calculated respectively to equation 2.7 and equation 2.8. Results for R_a is presented in table 4.4 and for R_q in table 4.5.

Table 4.4: Average roughness, R_a , for the concrete samples used in ice-concrete abrasion experiments. Roughness is presented before abrasion, 0 m, and after abrasion, 500 m effective sliding distance. μ is the mean and σ the standard deviation.

C. Sample	R_a [mm]			
	Reference Points		Ice Exposed Points	
	0 m	500 m	0 m	500 m
STD9	0.040	0.043	0.047	0.051
STD12	0.039	0.043	0.037	0.043
STD6	0.049	0.042	0.043	0.041
D8.2	0.047	0.046	0.051	0.049
D4	0.069	0.068	0.088	0.078
D1	0.061	0.063	0.077	0.066
D2	0.041	0.043	0.053	0.056
D8	0.044	0.044	0.046	0.047
D2.2	0.068	0.073	0.069	0.068
D7	0.089	0.086	0.084	0.075
D7.2	0.052	0.051	0.049	0.049
D6.2	0.047	0.039	0.046	0.043
D6	0.048	0.046	0.049	0.057
D1.2	0.067	0.079	0.092	0.111
D4.2	0.043	0.054	0.044	0.051
$\mu \pm \sigma$	0.054 ± 0.014	0.55 ± 0.015	0.058 ± 0.018	0.059 ± 0.018

Table 4.5: Mean square root roughness, R_q , for the concrete samples used in ice-concrete abrasion experiments. Roughness is presented before abrasion, 0 m, and after abrasion, 500 m effective sliding distance. μ is the mean and σ the standard deviation.

C. Sample	R_q [mm]			
	Reference Points		Ice Exposed Points	
	0 m	500 m	0 m	500 m
STD9	0.073	0.068	0.069	0.066
STD12	0.072	0.072	0.069	0.066
STD6	0.082	0.072	0.061	0.063
D8.2	0.047	0.046	0.072	0.070
D4	0.100	0.101	0.092	0.087
D1	0.096	0.089	0.106	0.073
D2	0.086	0.087	0.065	0.072
D8	0.076	0.070	0.069	0.054
D2.2	0.090	0.080	0.064	0.065
D7	0.118	0.143	0.061	0.039
D7.2	0.076	0.106	0.065	0.044
D6.2	0.086	0.091	0.061	0.039
D6	0.090	0.078	0.078	0.069
D1.2	0.105	0.096	0.108	0.127
D4.2	0.070	0.072	0.065	0.070
$\mu \pm \sigma$	0.087 ± 0.014	0.087 ± 0.020	0.074 ± 0.016	0.069 ± 0.020

4.6.4 Concrete Samples after Ice Exposure

Concrete samples that have been subjected to ice abrasion are presented in figure 4.21. Figures 4.21a to 4.21e are samples having the greatest abrasion rate of the three tested concrete samples within each ice making procedure. Greatest abrasion rate was found as an average between the two calculation methods introduced in section 3.6.2. The ice exposed surface, see figure 3.16, can be, in contrast to the grayish color along the edges, seen as a darker color in the sample center.



(a) Concrete sample STD9 exposed to ice made after procedure 1.



(b) Concrete sample D8.2 exposed to ice made after procedure 2.



(c) Concrete sample D2 exposed to ice made after procedure 3.



(d) Concrete sample D7 exposed to ice made after procedure 4.



(e) Concrete sample D6 exposed to ice made after procedure 5.

Figure 4.21: Concrete samples after ice exposure. Samples have the highest abrasion rate within each ice making procedure, average of both method 1 and 2. Polished darker area has been exposed to ice.

4.6.5 Friction, Load and Temperature Variation

Data Histograms of the load, temperature and friction have been plotted with MATLAB®. Concrete samples that had the highest abrasion rate for each procedure have been selected and are presented in the following. All data was logged with 10 Hz. The insertion of new ice samples in the ice container is clearly seen as a short duration of high friction variations, See for example figure 4.22b at 85 min.

Friction

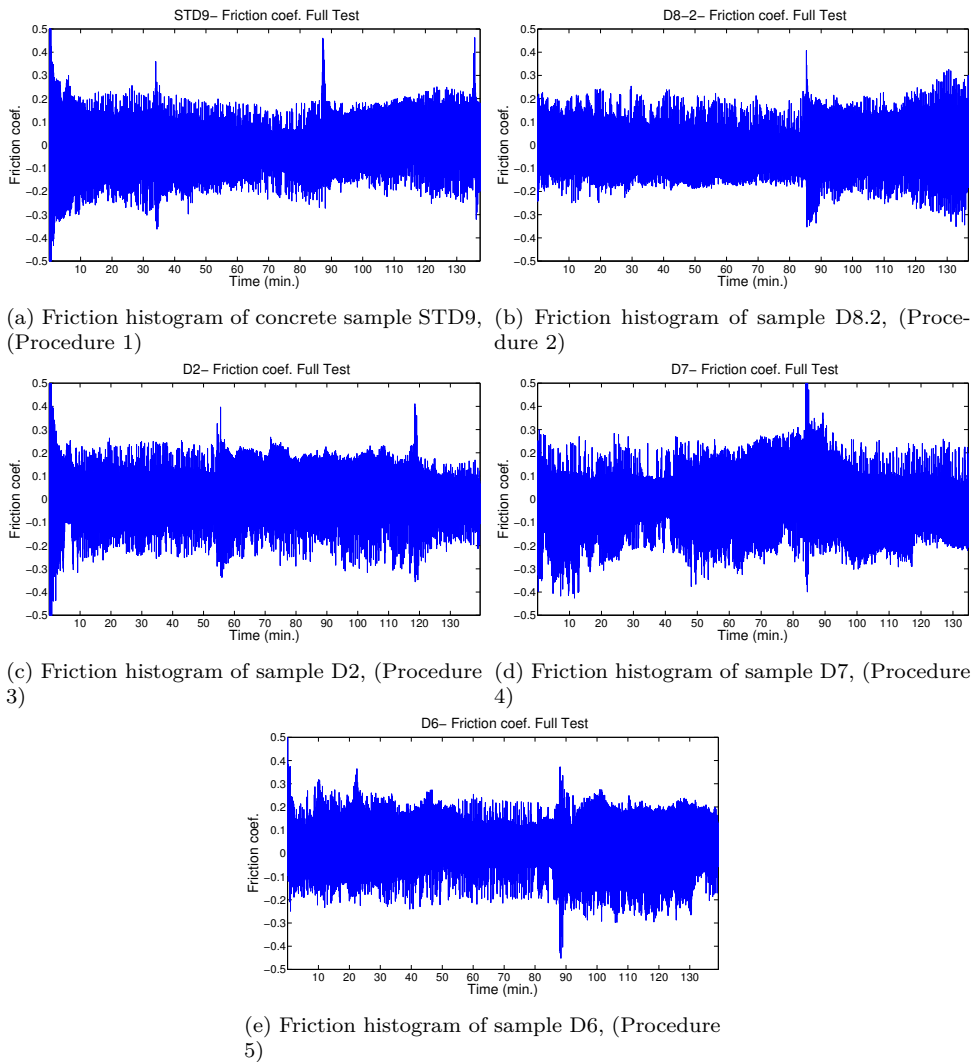


Figure 4.22: Comparison of friction coefficient during ice-concrete abrasion.

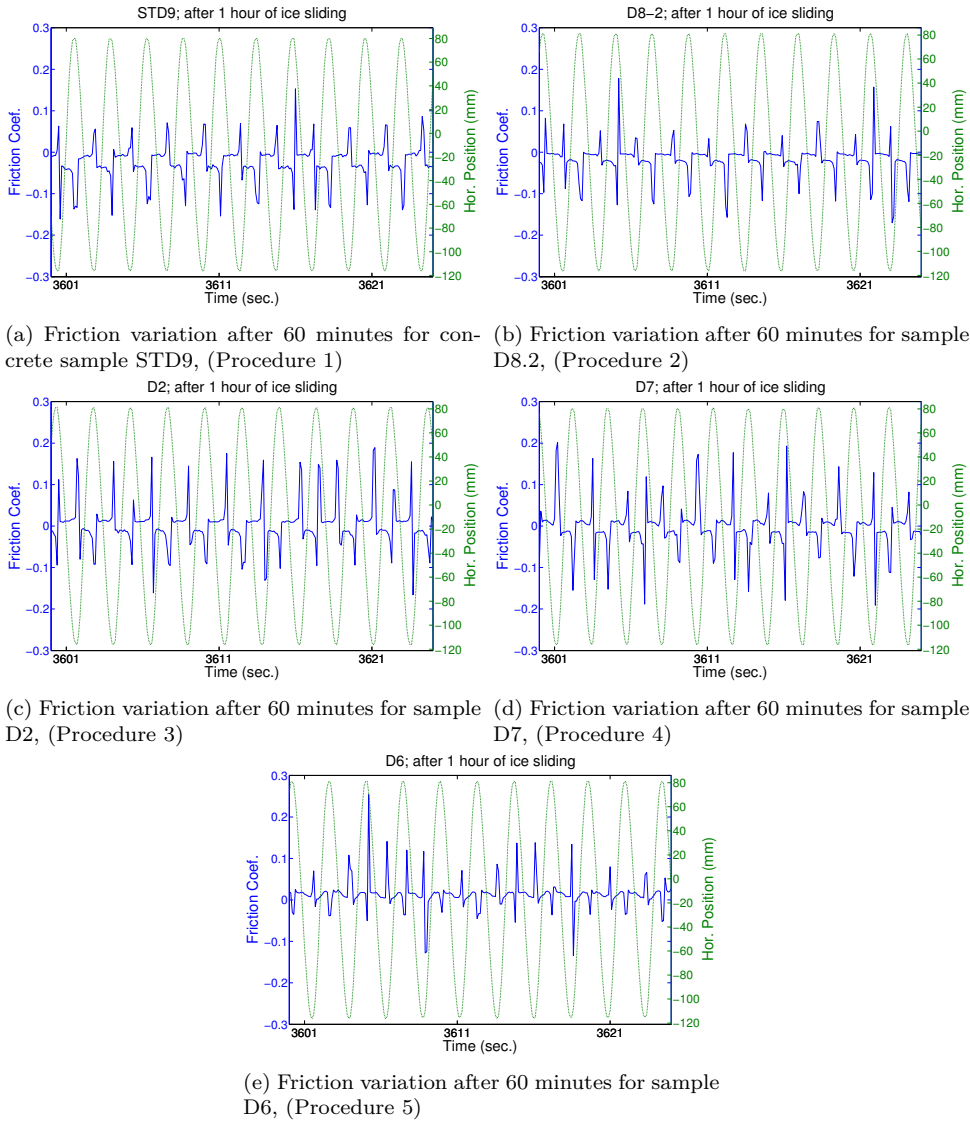
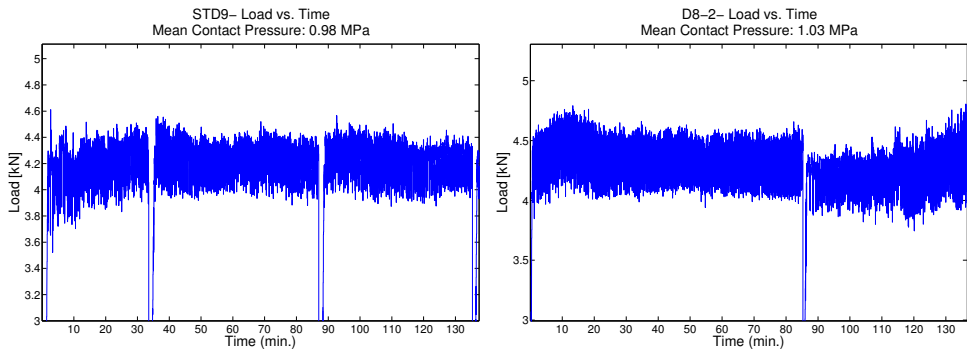
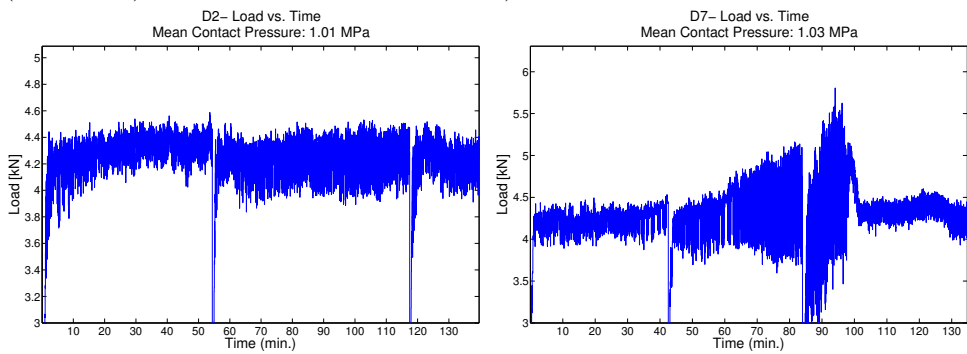


Figure 4.23: Comparison of friction coefficient variations after 60 min of ice abrasion. Ice movement = green line.

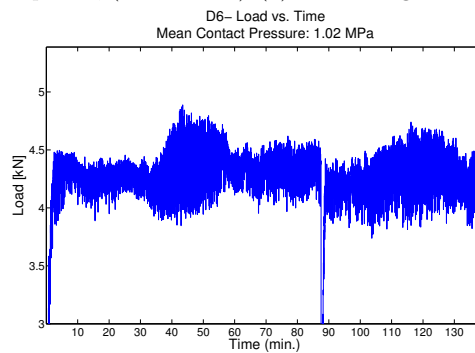
Load



(a) Load histogram of concrete sample STD9, (b) Load histogram of sample D8.2, (Procedure 1)



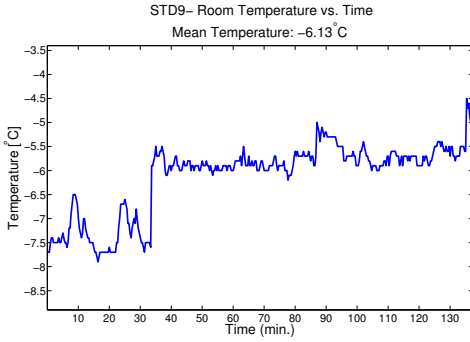
(c) Load histogram of sample D2, (Procedure 3) (d) Load histogram of sample D7, (Procedure 4)



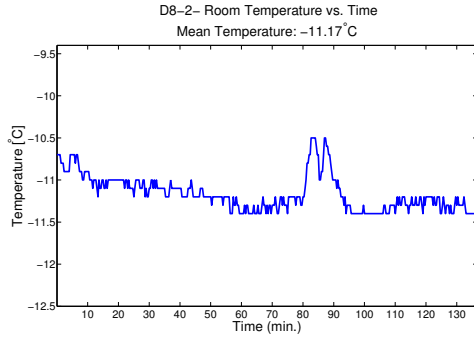
(e) Load histogram of sample D6, (Procedure 5)

Figure 4.24: Comparison of forces acting on concrete sample during ice-concrete abrasion. Load is presented for each of the five ice making procedures.

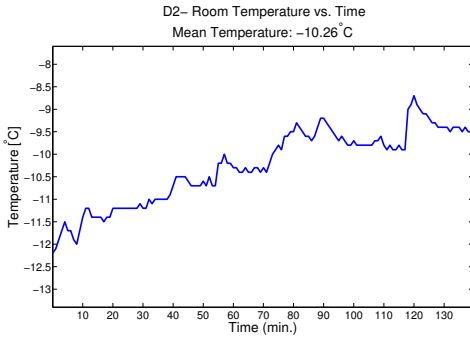
Room Temperature in Cold-lab



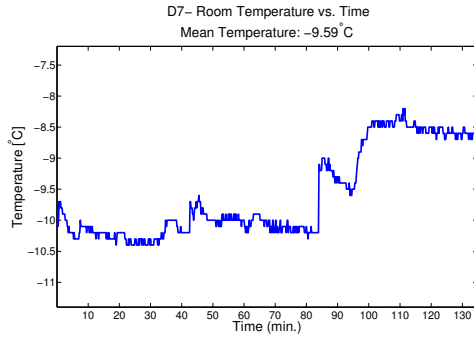
(a) Room temperature histogram of concrete sample STD9, (Procedure 1)



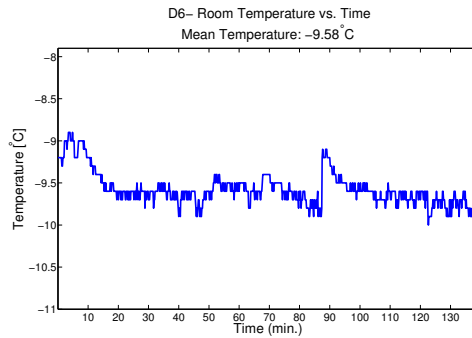
(b) Room temperature histogram of sample D8.2, (Procedure 2)



(c) Room temperature histogram of sample D2, (Procedure 3)



(d) Room temperature histogram of sample D7, (Procedure 4)



(e) Room temperature histogram of sample D6, (Procedure 5)

Figure 4.25: Comparison of room temperature during ice-concrete abrasion tests. Room temperatures are presented for each of the five ice making procedures.

Chapter 5

Discussion and Analysis

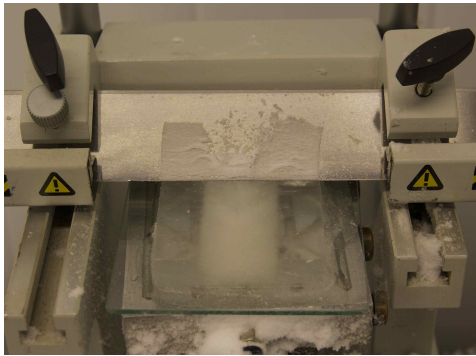
5.1 Ice Samples

As stated in the objective of this thesis, section 1.2, it is of interest to establish whether different qualities of fresh water ice can be used for computing abrasion on marine concrete structures. For that reason, five different procedures were developed to produce ice with dissimilar quality. The characteristics of the ice samples made after the various procedures, presented in section 3.1, will in the following be discussed. It will be concluded on whether the developed procedures made ice samples with differing qualities or not. The expected mechanical properties of the produced ice will also be discussed. For simplicity, procedure 1, procedure 2, ..., procedure 5 will respectively be referred to as p1, p2, ..., p5

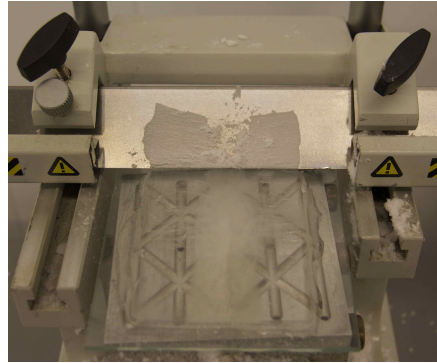
There is an apparent visual difference between the produced ice samples, seen in figure 4.1. A comparison of the thin sections revealed an evident difference in ice texture between p1, p3, p4 and p5. The density and porosity measurements conducted have shown that p4 and p5 produced ice sample porosities different from p1, p2 and p3. During the thin section preparation, it was observed how the procedures had apparent different characteristics, see figure 5.1. Both p1 and p2 showed collapsing center parts due to concentration of precipitating air during freezing. The cohesive edge part of p2 is wider than p1, which is reasonable, as p2 is wider than p1. Having the highest porosity, p4 had a dispersing characteristic and had to be treated very carefully during preparation, as p4 became very fragile for small thicknesses. Cohesive slices for both p3 and p5 indicates a homogeneous ice texture. The continuously stirring of the water in p3 causes the air in the water to be mixed, and precludes air to be dissipated towards cylinder center. The slice from p3 appears to have some caving, while p5 seems completely intact. This could stem from the higher porosity and dissimilar ice texture of p3.

5.1.1 Procedure 1 vs. Procedure 2

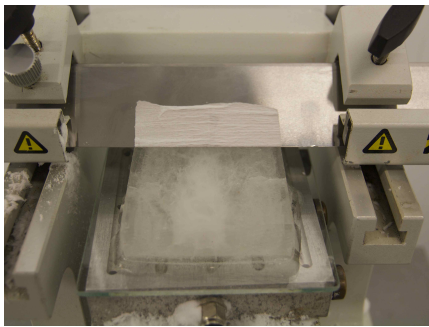
The size difference between p1 and p2 is hard to notice in figure 4.1b, but the purpose of p2 was exclusively to increase the diameter compared to p1. From the thin section and density investigations it can be concluded that p2 differed solely in sample width from p1. Similarities between the samples p1 and p2 and the samples in the pre-study were seen for both ice texture and density. An exception was seen for the thin section presented in figure 4.6a, showing smaller grains than the other top horizontal sections. This is most likely caused by retrieval of ice located close to the top of the ice sample. Freezing begins at the top and creates primary ice, which has a different texture than the predominant underlying secondary ice. Ice sample sections should be cut out from approximately the same place in the ice sample, in order to have a good comparison base. Despite this, the ice making procedure, where tap water is frozen in a plastic tube, has been repeatable for the samples in this thesis.



(a) Collapsed center of sample 16's vertical section, (Procedure 1)



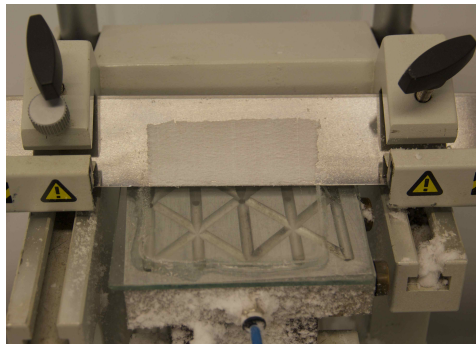
(b) Collapsed center of sample a25's vertical section, (Procedure 2)



(c) Collapsed center of sample b7's vertical section, (Procedure 3)



(d) Collapsed center of sample c13's vertical section, (Procedure 4)



(e) Collapsed center of sample d5's vertical section, (Procedure 5)

Figure 5.1: Comparison of vertical sections during thin section preparation. Length axis of the ice sample was oriented orthogonally to the blade. Samples have been shaved once with the microtome.

5.1.2 Mechanical Properties of Ice

As presented in section 2.1.7, mechanical properties of ice alter with different values of porosity, brine content, grain size and orientation. Investigations of the different ice samples have shown apparent differences in ice texture and porosities. It can therefore be assumed that the mechanical properties of the ice samples also differ.

According to figure 2.5, it is assumed that p3 samples have greatest ice strength, as the freezing temperature was lowest for p3 (-20 °C). The room temperature during abrasion test conduction however is the same for every test (-10 °C). The temperature at the concrete surface is somewhere around 0 °C. These higher temperatures will heat the ice sample p3 and thereby lower its strength accordingly to figure 2.5. In order to determine the influence of ice temperature on ice-concrete abrasion, abrasion tests with different temperatures should be conducted.

Vertical air pillars, as seen in figure 5.2, were spread over the ice floe in FRY-SIS. The amount of air in the ice made after p5 was seemingly smaller than in the other ice samples. As p5 ice was frozen in a 1 m³ water tank, air could dissolve in the water as freezing proceeded and expelled air. Also, no concentration of air, as in the tubes, could occur. The small amount of air is reflected in the calculated porosity. As the porosity of p5 was lowest, it is, according to figure 2.7, expected that the Young's modulus of p5 is greatest. The large grains that were seen in the thin sections of p5 resembles mono-crystalline ice. According to Hobbs (1974), mono-crystalline ice has a higher strength than poly-crystalline ice.

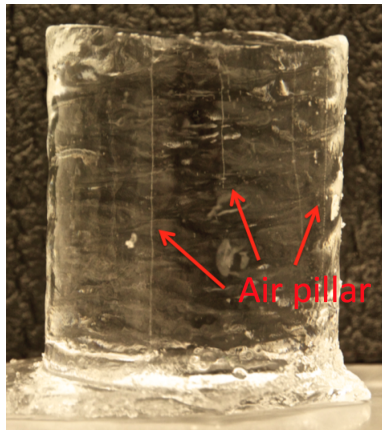
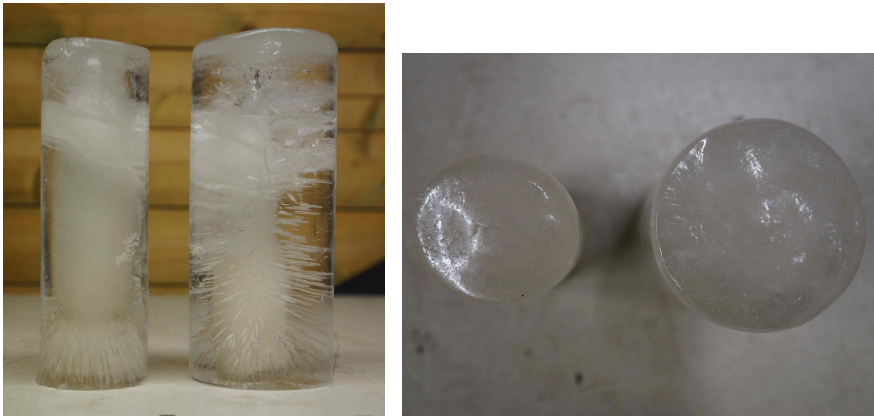


Figure 5.2: Air pillar in ice sample made after procedure 5.

5.1.3 Shrinkage

Due to unforeseen downtime of the abrasion rig, some ice samples had to be stored for a longer period of time. Samples were stored free to air on a shelf located in the cold-lab, next to the abrasion rig. With time, it was observed that the ice samples had shrunk. A sample stored for 34 days can be seen in contrast to a sample that has not been stored in figure 5.3. The shrinkage was recorded for eight samples made with p2 and calculated to be an average of 0.61 mm/day. The shrinkage was presumably due to sublimation of ice caused by the constant air circulation in the cold-lab by the cooling fans and the repeatedly opening and closing of the laboratory door. As soon as this was detected, the samples were stored in the cylinders until usage. This eliminated the negative shrinking effect. As an alternative, if the tubes are needed, the samples could be covered with for example a bucket. This would most likely reduce shrinkage and free cylinders to produce more ice samples. An uncontrolled reduction in sample size, is another variable in the ice-concrete abrasion problem and could inflict abrasion results. It is therefore recommended in future studies to avoid ice sample storage in the cold-lab.



(a) Ice Sample stored for 34 days (left) and not stored (right) (b) Top view: Ice Sample stored for 34 days (left) and not stored (right)

Figure 5.3: Ice sample made after procedure 2 illustrating shrinkage from storage. Ice sample which hasn't been stored has a diameter $\phi = 47$ mm while the sample stored has $\phi = 73.4$ mm.

5.2 Analysis of Ice-Concrete Abrasion Studies at NTNU

As part of a quality assurance, the repeatability of the abrasion rig was investigated. It was desired to compare the results obtained in this thesis to earlier results obtained from the same abrasion rig. Test conductions, found in the thesis of Møen (2009), Bøhn (2011) and Kirkhaug (2013), were determined before abrasion testing started and are found in table 3.1. As seen in table 5.1, the test conditions for the various theses vary. The measured mean abrasion rates vary as well.

Table 5.1: Comparison of ice-concrete abrasion studies at NTNU. - = unknown.

Variable	Møen (2009)	Bøhn (2011)	Kirkhaug (2013)	Greaker (2014)
Concrete type	w/c=0.6, w/ air	w/c=0.6, w/ air	B60	w/c=0.6, w/ air
Saw/Casting surface	Casted	Sawed	Sawed	Casting
Honed	-	-	✓	✓
Con. cracking	-	✓	✓	No
Saturated	-	✓	✓	No
Ice Sample	Fixed Tube	-	Fixed tube	p1
Ice sample storage	-	-	Yes	No
Vertical load [kN]	4.3	4.3	4.3	4.5
Sliding velocity [cm/s]	17	10	16	16
Eff. sliding distance [m]	185	500	1250	500
Pego Temperature [°C]	-10	-10	-10	-10
Julabo 2000 temp. [°C]	-	-	12	11
Measuring technique	-	Unlike	~ m2	m1/m2
# tested samples	2	1	2	3
Abrasion rate [mm/km]	0.216	0.124	0.09	0.002/0.023

Unfortunately, it was not possible to obtain complete details on every variable and condition used in these tests. Hence it can not be determined whether the conditions used in the earlier theses were completely equal with the present test. For example it was not clear whether the saw surface or casting surface was submitted to abrasion. A honed surface could differ, as there was no information about how much the samples have been honed. Other conditions could have been left out unintentionally. It is unknown which parameters that influence abrasion results. Therefor it is uncertain if the results obtained in this thesis can be compared to the earlier results. However, the abrasion result from this thesis differ from those in earlier theses. The difference in the abrasion rate between the theses could be explained by the difference in test conditions seen in table 5.1. Therefore it can not be concluded on whether the abrasion rig is repeatable or not. When comparing abrasion results, it is important to have as similar experimental conditions as possible.

5.2.1 Analysis of earlier Ice-Concrete Abrasion Results

The abrasion results obtained in earlier theses from the ice-concrete abrasion rig located at NTNU have been analyzed. The purpose has been to survey any possible spread in the abrasion results caused by the experimental set-up. The survey of these results has been used to conclude on the accuracy and repeatability of the measurement procedure.

Abrasion Rate vs. Concrete Type

In figure 4.17 it can be seen how abrasion rate varies with concrete type for three different test conditions. Mean abrasion rate is dependent on test conditions whereas the order of concrete type ice resistance is constant for varying test conditions. Only exception is seen for the densit specimen in figure 4.17c. The densit material has the lowest mean abrasion rate in figures 4.17a and 4.17b, thereby being the strongest material. However the opposite is observed in figure 4.17c, where the densit concrete has the highest mean abrasion rate, thereby being the weakest material. Given the rather high standard deviation in figure 4.17c and the negative abrasion rate in figure 4.18c, it is reasonable to assume that there has been an error and exclude the irregularity in figure 4.17c. Taking this observation into account, the results from earlier studies are showing a coherent pattern. The abrasion rates differ from type of material, whilst the material abrasion resistance persists with altering contact pressure and sliding velocity. It should be addressed that the number of data is low. In order to get a good statistically representation, additional tests should be performed. In figure 4.17a one can see how the results from Møen (2009) have a larger deviation than the results from Kirkhaug (2013). This could indicate that the precision in measurements are dependent on the operator.

Abrasion Rate vs. Relative Difference

As seen in figure 4.18, each mark, representing the combination of concrete specimen and test condition, are showing close to constant mean abrasion rate for two parallel samples for all sliding distances. This finding indicates that there is a linear relation between the mean abrasion and sliding distance, which is coherent with literature, (Hanada et al., 1996; Saeki, 2010). Identical abrasion rates also indicate that the measurement accuracy is satisfying.

A further observation is that the relative difference has a decreasing trend with increasing abrasion rate. This can be perceived as that accuracy increases for greater abrasion. The fact that results from 0-2500 m effective sliding, figure 4.18b, shows the lowest spread in relative difference, supports this conclusion. As presented in table 5.2, the weighted deviation of the measurements is relatively large. Therefore, measurements taken on specimens with a high abrasion resistance (= low abrasion rate), would have a lower accuracy. The densit concrete specimen demonstrates this effect in figure 4.18, especially for the test condition 25 cm/s and 1 MPa. Except for some outliers, the majority of results with a high accuracy have a mean abrasion rate >0.4 mm/km. In order to obtain accurate results, it is therefore

recommended to abrade concrete specimens an average of $0.04 \text{ mm/km} \times 1.25 \text{ km} = 0.05 \text{ mm}$.

In accordance with Archard (1953), figure 4.18 shows that all concrete specimen undergoing contact pressure = 0.5 MPa had lower abrasion rates than those undergoing a contact pressure of 1 MPa and equal sliding velocity. This is consistent to literature in table 2.1, though according to Itoh et al. (1988) wear rate would double when contact pressure is doubled. This was observed for the B70 specimen in figure 4.18a and for some other specimens, but not to a magnitude that could indicate a clear correlation.

5.3 Abrasion Measurement Set-Up and Calculation Procedure

As highlighted in section 5.2, the abrasion rig test conditions and measured mean abrasion rates differed between the earlier ice-concrete abrasion studies at NTNU. The measured abrasion rate for p1 with calculation method 1 was more than 108 times lower than the the result by Møen (2009). An investigation of the accuracy of the abrasion depth measurement set-up and the method used to calculate abrasion rate was commenced in order to determine the reliability of the abrasion results.

5.3.1 Equipment

The Mitutoyo Corp. 543-250B ID- C112B digital indicator was extremely sensitive to any movement. It showed different readings when left for a couple of minutes at the same grid point. When moving the needle up and down, the instrument showed a different value. The different values shown by the instrument appeared to be random. The deviation occurring when left for some time was mostly ± 0.003 mm, which is the indicators deviation given by the manufacturer. The reason for the deviation occurring when lifted and released could be explained by a slack in the measuring system. Any slack would allow for micro movements in either direction. With the concrete surface given roughness, the needle head could shift to any side of a micro knob and thereby give a different reading. It could also have significantly influence for situations seen in figure 5.4.



Figure 5.4: Mitutoyo indicator needle hanging on a cavity wall. The needle tip measures 1.8 mm in diameter.

In order to retrieve the 110 grid points presented in section 3.6.1, a total of 160 rotations in y-direction and a total of 910 rotations in x-direction is needed. The relatively large number of rotations increases the probability for random errors. Human error can easily occur and must be considered as likely. It Slack in the system was observed as the coordinate table didn't start to move before half a

rotation when direction was changed. That each grid point was hit perfectly is very unlikely, as the starting point for each rotation was estimated visually. For example handle grip pointing upwards. In addition the concrete sample had one side which was pebbled and made it difficult to obtain a good starting position for the initial measurement. Small differences could have large influences as is illustrated in figure 5.4. A small shift forward or backward would cause that the needle head either ended up at the bottom or at the top of the cavity. Systematic errors must also be considered. A skewness in the table on which the apparatus rested is likely but was not investigated.

5.3.2 Accuracy of Measurement Set-Up

Sætre (2014) measured the surface of a B70 concrete sample a total of six times. The standard deviation for each of the 110 grid points were calculated and the average standard deviation of these points was 0.0059 mm. This can be interpreted as that when point $p_{x,y}$ is measured, the same point after ice exposure, $\hat{p}_{x,y}$, is expected to have an average deviation of 0.0059 mm caused by errors in the measurement procedure. This is twice the deviation of 0.003 mm given by the digital indicator, (Mitutoyo, 2005). It can be concluded that errors are caused by other factors than the deviation of the measuring instrument. The results from the six measurements gave a weighed standard deviation of 0.0004 mm. The weighted standard deviation was calculated after equation 1.36 in Lyons (1991) and is expressed as:

$$1/\sigma^2 = \sum (1/\sigma_i^2) \quad (5.1)$$

The low weighted standard deviation indicates that the measurement procedure is repeatable.

5.3.3 Calculation Method 1 vs. Method 2

Figure 4.20b shows that the two methods for calculation of the abrasion rate were not correlated. This indicates that the methods were dissimilar and were calculating abrasion rate with different approaches. It was however not possible to reveal which of the methods was more correct or if they were both equally wrong. It has been attempted to investigate the influence of the uncertainties and evaluate the accuracy of the calculation methods in order to conclude on which method that might have given more accurate results. The two methods were based on different weighting of errors. Method 1 assumed that most of the measurement errors were random, while method 2 assumed that most of the errors were systematic. In order to determine which of the two methods were closer to the real value, the standard deviations of the reference points for each concrete sample have been compared before and after abrasion.

$$\sigma_{ref} - \hat{\sigma}_{ref} = R \quad [\text{mm}] \quad (5.2)$$

Where σ_{ref} is the standard deviation of the reference points before abrasion and $\hat{\sigma}_{ref}$ is the standard deviation of the reference points after abrasion. R is the difference between the deviations. The standard deviation of the grid points will consist of the concrete surface roughness, the indicators deviation, random errors and systematic errors. As the reference points are not exposed to ice, it can be assumed that the roughness before abrasion is identical to the roughness after abrasion. The deviation of the digital indicator will be the same for each measurement. Therefore it can be assumed that the deviation caused by the surface roughness and the instrument are not affected by the measurement set-up and assumed constant. Other errors occurring in the system for various reasons are denoted ϵ and can differ.

$$(\epsilon + c) - (\hat{\epsilon} + c) = R \quad [\text{mm}] \quad (5.3)$$

$\hat{\epsilon}$ is any error after abrasion and c is the constant deviation in the system, namely surface roughness and indicator deviation. We can now divide the errors, ϵ into systematic, $\epsilon_{systematic}$ and random errors, ϵ_{random} and equation 5.3 becomes:

$$(\epsilon_{systematic} + \epsilon_{random}) - (\hat{\epsilon}_{systematic} + \hat{\epsilon}_{random}) = R \quad [\text{mm}] \quad (5.4)$$

Lyons (1991) states that systematic errors can cause the measurements to be offset from the correct value, even though the individual results can be consistent with each other. Random errors, on the other hand, will produce different values of the measured height of point $p_{x,y}$ in a series of repeated measurements. Assuming consistent systematic errors:

$$\epsilon_{systematic} = \hat{\epsilon}_{systematic} \quad [\text{mm}]$$

Equation 5.3.3 becomes:

$$\epsilon_{random} - \hat{\epsilon}_{random} = R \quad [\text{mm}] \quad (5.5)$$

If

$$R \approx 0$$

then the system has prevailing systematic errors, otherwise random errors are to be assumed predominant. The standard deviation of the reference points before, $p_{ref,y}$, and after ice exposure, $\hat{p}_{x,y}$ was calculated for all the tested concrete samples. From all these standard deviations, the weighted standard deviation was calculated according to equation 5.1 and are presented in table 5.2.

Table 5.2: Comparison of weighted standard deviations. Equation 1.36, (Lyons, 1991)

Before abrasion, σ_{ref}	After abrasion, $\hat{\sigma}_{ref}$
0.019	0.019

There is no difference between the standard deviations of the reference points and emphasizes that the errors in the system are systematic. Therefore it is recommended to calculate abrasion rate after method 2. Additionally, the difference between the weighted mean reference point height before and after ice exposure for all concrete samples was calculated to be:

$$\Delta\bar{p}_{ref} = |\bar{p}_{ref} - \tilde{p}_{ref}| = |-0.022 - (-0.019)| = 0.003 \text{ mm} \quad (5.6)$$

Where \bar{p}_{ref} is the weighted mean reference point height before abrasion and \tilde{p}_{ref} is the weighted mean reference point height after abrasion calculated with equation 1.35 in (Lyons, 1991):

$$a = \sum(a_i/\sigma_i^2) / \sum(1/\sigma_i^2) \quad (5.7)$$

Where a is the best estimate of a set of answers a_i with different errors σ_i . Equation 5.6 shows that the difference between the mean reference point height is equal to the deviation of the measuring instruments. This indicates that, despite the discussion in section 5.3.1, the measurement procedure can be used to measure the surface of the concrete sample. The recordings from the digital indicator are not random numbers but in fact surface heights relative to a given starting point. However, it is strongly advised to strive towards a measurement and calculation procedure in which an optical surface scanner is implied, see discussion by Sætre (2013). This would most likely improve the accuracy and reliability of the measurements greatly.

5.4 Concrete Sample

Concrete sample that had the greatest abrasion rate for each of the ice making procedures are presented in figure 4.21. As explained earlier, ice exposed surface can be seen as a darker color in the sample center, in contrast to the grayish color along the edges. The samples have been stored in room temperature free to air for several days before the pictures of the concrete samples were taken. Therefore, the darker color is not believed to be moist. It is reasonable to assume that the darker polished area is a result of a change in the surface topography caused by ice abrasion. During the abrasion test conduction, small particles could be felt on the concrete sample surface and were presumed to have a diameter ≈ 0.5 mm. The diameter of the particles was unfortunately not measured and is only a memory based estimate. Loosing of aggregate stone, as illustrated in figure 2.9, was not observed during any of the conducted experiments.

5.4.1 Profile Roughness

The profile roughness was derived from the same measurements used to calculate abrasion rate. An important observation in section 5.3.3 was that the surface roughness of the concrete sample could be assumed constant. It can thereby be concluded that surface roughness does not influence the measurement set-up accuracy. The deviation caused by any surface roughness will be equal for all measurements, provided no alteration of the surface has occurred. The conclusion is that even with a 100 % precise surface roughness measurement the overall accuracy of the measurement set-up wouldn't get better. The fact that the difference in the weighted mean reference point height was 0.003 mm and equal to the deviation of the indicator confirmed this observation.

The mean square root profile roughness parameter, R_q , was greater than the average roughness, R_a . Compared to parameter R_a , parameter R_q is more sensitive to deviations from the mean point height. R_q having being greater than R_a , could indicate that there are greater variations in the topography of the concrete surface than given by R_a . It is important to address the fact that the surface roughness has been calculated from $2 \times 70 = 140$ ice exposed grid points. These points are situated ± 20 mm in y-direction and ± 10 mm in x-direction from each other, see red dots in figure 5.5. As the figure illustrates, surface roughness characteristics can be missed, due to the rough grid point mesh and the heterogeneous nature of concrete. A finer mesh would catch more varieties in the topography of the concrete, but would also increase risk for errors and prolong measurements. It is therefore recommended to investigate concrete surface topography with a scanner, (Sætre, 2013).

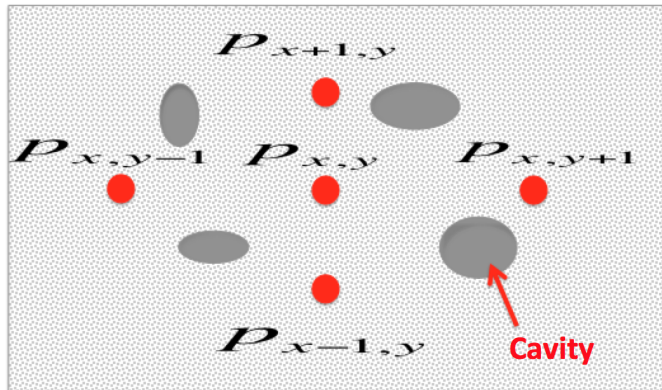


Figure 5.5: Illustration of how tops and valleys (grey spots) can be missed due to the rough mesh of grid points (red dots) $,p_{x,y}$.

5.5 Ice-Concrete Abrasion Results

The results from the conducted ice-concrete abrasion experiments presented in table 4.3 will be discussed in the following. The discussion in section 5.3.3 concluded that abrasion rates are to be calculated after method 2. Hence, the variation of abrasion rate as a result of differing ice quality will only be discussed for the rates obtained from calculation method 2.

5.5.1 Abrasion Rate Comparison

The abrasion rates obtained from the conducted experiments were seemingly smaller compared to earlier thesis at NTNU. Results from Kirkhaug (2013) are showing much lower abrasion rates than Møen (2009) and Bøhn (2011). Kirkhaug however performed abrasion experiments on concrete with different qualities. Table 14, (Kirkhaug, 2013), shows that both the concrete strength and density of the w/c=0.6 concrete was lower than for all specimens tested by Kirkhaug.

Section 5.3 concludes that the measurement set-up is accurate and repeatable. In order to discuss if the results obtained in this thesis are reflecting real abrasion, the results are compared with the model of Huovinen (1990). The strength of the concrete used in this thesis was measured to be $f_{cm} = 50.7$ MPa, which is the same as a B45 concrete. According to equation 2.10 presented by Huovinen (1990), the abrasion rate, b , would be expected to be:

$$b = \frac{3}{50.7} \times 0.5 = 0.03 \text{ mm/km} \quad (5.8)$$

The mean abrasion rate for the samples abraded with ice after p1 - p4 was 0.027 ± 0.084 mm/km. As explained in section 2.3.3, the equation presented by Houvinen is derived from empirical relations. The similarity between the rate found in equation 5.8 and the abrasion rate measured is noteworthy. Having results obtained in a laboratory similar to field results is desirable. If the empirical model by Houvinen is accepted as true for model abrasion, the values obtained in this thesis are to be considered more realistic than the results from earlier theses. However, this is conflicting with other studies, saying that concrete strength has no affect on abrasion rate, (Saeki, 2010). Also, the model by Houvinen is a simplification of equation 2.9 by Archard (1953), not accounting for any ice properties or contact pressures. The reason for the difference in the results between the theses can be many and some are highlighted in the earlier section 5.2. Due to the many variables further investigations are needed on the subject.

It is noteworthy to observe how the thin sections of p3 resembles the thin sections of sea ice, see figure 2.4b. The thin sections for p1, p2 and p4 have somewhat similar characteristics as for that of sea ice, that being different grain size distributions and orientation. Relations between ice texture and abrasion could hence be drawn. The crystal texture of p5, presented in section 4.2.5, is neither resembling

texture seen for fresh water, figure 2.4a, nor from sea water, figure 2.4b. The fact that mean abrasion rate from p5 is an outlier in figure 4.20a, underpins that the abrasion rate is influenced by ice texture. This observation can be valuable for further investigations on ice quality effect on ice-concrete abrasion. The influence of ice texture on ice-concrete abrasion should be investigated further.

5.5.2 Abrasion Rate vs. Ice Quality

In figure 4.19 it can be seen how abrasion rate varies for each ice procedure presented in section 3.1. Due to the high porosity of p4, it was expected to have the lowest abrasion rate. However this could not be observed in figure 4.19. Carbonated water was used in p4 to produce ice with a large number of gas pockets. First after test conduction, the effect carbon dioxide has on concrete was discovered. The carbon-dioxide in the mineral water will dissolve the calcium-hydroxide in the concrete and cause leaching, (Norcem, 2014). Due to the relatively high w/c ratio, the concrete used in this thesis would be susceptible for leaching. The abrasion tests conducted had however a rather short duration time and it is unknown if concrete leaching occurred. The difference in mechanical properties for the ice samples discussed in section 5.1.2 could explain the variations in the abrasion rates. It is left to conclude that ice-concrete abrasion is a complex field of study and abrasion as a function of ice porosity should be investigated further.

The fact that p3 had a higher abrasion rate than the other procedures where ice samples are made in tubes and frozen at $-10\text{ }^{\circ}\text{C}$, could indicate an influence of temperature on ice-concrete abrasion. As has been discussed earlier, ice strength increases for lower temperatures. Also the smaller grain sizes observed for p3 could have an influence on abrasion rate. From theory it is known that grain size affect the uniaxial tensile strength and the compressive strength of ice. The relation between compressive strength of ice and abrasion should be investigated further.

As discussed in section 5.1.2 the large grains seen for p5 resembled mono-crystalline ice. This could be one of the factors causing p5 to exert the highest mean abrasion rate. P5 has also the lowest measured porosity. According to the discussion on p4, abrasion as a function of ice porosity should be investigated further.

Wear and abrasion theory discusses that for various properties of concrete (aggregate size, compression strength of stone, concrete surface, etc...) abrasion rate varies. The same conclusion was drawn in section 5.2.1. Results from Kirkhaug (2013) and Møen (2009) showed that the mean abrasion rate for different types of concrete had a variation $\approx 0.02 - 0.09\text{ mm/km}$. When the same comparison is made, but now for different ice qualities, an almost identical variation of the mean abrasion rate can be seen, figure 4.19b. The variation of the mean abrasion rate for different ice qualities was $\approx 0.02 - 0.07\text{ mm/km}$. The similarity of the abrasion rate variations could indicate that ice quality in fact has an influence on ice-concrete abrasion. If variations in abrasion rate caused by differing concrete types is to be acknowledged, due to the similarity of the abrasion rate span, variations in abra-

sion rate with different ice qualities should be acknowledged as true as well. It is important to address that the variation seen for the results obtained in the present thesis are only from a 5×3 ice sample population. It has not been attempted to produce ice of equal quality to that of sea ice. Therefore it can not be derived any conclusion on whether abrasion rate would differ with natural fresh water ice and natural sea ice. The laboratory tests performed have however shown that the different ice textures and densities of the ice produced have given a variation in abrasion rate.

The variation for the different ice qualities show a larger deviation for each procedure than the variation in Kirkhaug (2013) results. This is most likely due to the short sliding distance. As concluded in section 5.2.1, it was recommended to ensure a minimum abrasion depth of 0.05 mm in order to increase measuring accuracy. As has been highlighted earlier, the concrete samples in this thesis did not abrade as much as in earlier theses. Therefore it is recommended to conduct experiments with a longer ice sliding distance.

5.5.3 Effect of Volumetric Expansion

P2 differed solely from p1 in sample diameter size. The purpose with p2 was to investigate the effect of the volumetric expansion addressed in the pre-study. As can be seen in figure 5.6, p1 showed a clear deformation with cracking of the sample after it had been subjected to abrasion. As the ice sample container measures 73.4 mm in diameter, p1, having a diameter of 70 mm, can be forced to deform by the vertical load exerted on it. P2, fitting perfectly in the ice sample container, can't deform. After ice-concrete abrasion, all p2 samples had equal appearance as the p2 sample seen in figure 5.6. It can therefore be concluded that by preventing the ice sample to expand in the container, it will not crack.



Figure 5.6: Comparison of intact p2 POM, $\phi = 73.5$ mm, sample (left) and broken p1, $\phi = 70$ mm, ice sample (right) after an ice-concrete abrasion test. Abraded surface on top.

Janson (1988) discusses the relation between energy dissipation of kinetic energy and abrasion rates. Where energy dissipation is associated with the breaking of ice. As p2 does not break during the abrasion test, it is to assume that the energy dissipation for p2 is different than for p1. This could be a reason for that p2 has the lowest abrasion rate calculated with method 2. This could also explain the difference between abrasion rates of seemingly equal ice quality. If there is a difference in ice sample diameter, the hypothesis of energy dissipation by Janson would govern different abrasion rates. Different sample diameter can be due to different thawing time. This observation should be investigated further.

5.5.4 Friction histogram

Compared to the friction coefficient from Kirkhaug (2013), a larger fluctuation can be observed for the friction coefficients recorded in this thesis. The concrete sample used to investigate friction by Kirkhaug (2013) was Rockbond concrete. The concrete had similar roughness parameters as the concrete investigated in this thesis. Due to the low grid point mesh and the omission of other surface characteristics, it is uncertain how descriptive the profile roughnesses are. It will therefor not be concluded on friction variations in regard to profile roughnesses.

Kirkhaug recorded data once per cycle, while this thesis records with a logging frequency 10 Hz. Some greater deviations can be seen in the histograms of Kirkhaug, reaching static friction peak values ≈ 0.2 . Similar peak values was observed in present thesis, only much more frequent. The reason for the absence of the higher static friction coefficients in the histogram by Kirkhaug was due to the lower logging frequency. A sampling rate of 10 Hz detects more of the friction variation. As mentioned in section 3.5.1, it was intended to investigate friction variations with a higher sampling rate. This would most hopefully detect the exact variation of the coefficient and allow for a better analyzation. The analyzation of friction is an important subject in the field of abrasion study and it is suggested that the intended investigation of the friction coefficient should be commenced in future work.

The comparison of the friction variations for 25 seconds in figure 4.23 show similar observations as in the pre-study. There is an apparent asymmetry in the dynamic friction. Other, similar, plots from various durations of the same experiment indicated variations of the time dependency of the dynamic friction coefficient of the type seen in figure 4.23. The coefficients can be very close to zero in one direction and either positive or negative in the other direction.

Dynamic friction for sample D6 in figure 4.23e was close to 0 and distinguished it self from the other recordings. Noteworthy is that D6, having the lowest porosity, also has the highest abrasion rate. This observation is not coherent with theory on the relation between friction and wear, (Fosså, 2008). However the variation seen in figure 4.23e must not be applied for the entire experiment. Friction variations are great and differs with time. It is once more recommended that further work should concentrate on the study of friction in relation to ice-concrete abrasion.

5.5.5 Load histogram

Theoretically, a vertical load of 4.3 kN would be equivalent to a contact pressure of 1 MPa. It was noticed that a vertical load in Labview of 4.3 kN would exert an average pressure on the concrete sample lower than 1 MPa. It was proven that the vertical load had to be 4.5 kN in order to obtain an average contact pressure of 1 MPa, see figure 4.24.

The magnitude of the load in the load fluctuated, but the response system managed to maintain an average contact pressure of 1 MPa. Noteworthy observation was the load histogram for p4 in figure 4.24d. After insertion of the second ice sample ($t = 42$ min), the load magnitude increased with time. After insertion of the third ice sample ($t = 85$ min), the increasing trend continued for approximately 10 minutes with large fluctuation until a sudden load drop to ≈ 4.3 kN. As p4 had a significant higher porosity than the other procedures, this could be the cause for the fluctuations and load build up. During experiment trial, it was noticed how the rig stuttered remarkably more than for the other ice procedures. Almost as the ice p4 was more ductile and stuck to the concrete sample as it was moving across the surface. Abrasion as a function of ice porosity seems to be a variable in need of further investigation.

During operations it was noticed that ice started to build up under the table holding the concrete samples. Melt water from the ice samples had sieved through a fault in the membrane surrounding the bearings and frozen around the vertical load-cells. This phenomena caused the load reading by the vertical load-cell A to diminish. The freezing of the load-cell A occurred for the later abrasion experiments. Ice build up occurred after some trial time, as enough water had to freeze around the load-cell. The counteract was to heat the load-cell with a industrial dry blower, see figure 5.7, which solved the problem temporarily. Before any further experiment conduction the abrasion rig should undergo maintenance.

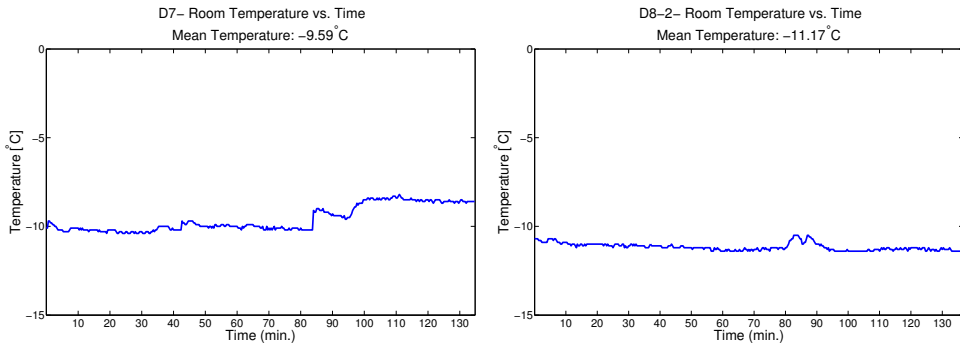


Figure 5.7: De-icing of load-cells. Industrial dry blower blowing air at a temperature of ≈ 150 °C at the load-cells seen under the table holding the bearings. Load-cell A to the right and load-cell B to the left.

5.5.6 Temperature histogram

The cold-lab had an average room temperature of approximately -10°C . Attention is directed to the misleading column names of the output file from Isabrasive-v3. The temperature histogram in the present thesis originates from the data in the column called "Reserve Temp wago 22" and was the same column the data used by Kirkhaug (2013) originated, referred to as room temperature in his thesis.

Deviation due to entering and exiting the cold-lab can be seen for some of the temperature histograms. For comparison reason, the axes of the temperature plots, figure 4.25, are set to be equal to the axes of the temperature histograms of Kirkhaug in figure 5.8. From figure 5.8 it can be concluded that there are less temperature variations than seen in Kirkhaug (2013). This observation can be seen for all the conducted ice-concrete abrasion experiments. It would however be of greater interest in future work to present the temperature recorded in the ice sample container. It is believed that data in column "Air Temp [C] wago 21" represents the temperature in the sample container. This would show temperatures experienced by the ice sample. As seen in theory, temperature influence ice properties greatly and could be an important variable in the ice-concrete abrasion problem.



(a) Room temperature variation of concrete sample D7 (b) Room temperature variation of concrete sample D8.2

Figure 5.8: Room temperature variation with y-axis equal to Kirkhaug (2013)

Chapter 6

Conclusions

The main objective of this thesis has been to investigate the possible effects of different ice qualities on laboratory ice-concrete abrasion tests. This has been done by altering the ice parameters and keeping other test conditions constant. In order to achieve the objective, supplementary investigations on the abrasion measurement set-up and calculation method have been commenced. In regards to the objective the main findings were:

- The laboratory tests conducted with ice produced in this thesis have given a variation in abrasion rates.
- The five procedures developed made ice samples with different qualities.

The main findings from the supplementary investigations were:

- The variation of abrasion rate caused by different ice qualities was similar to the variation of abrasion caused by different concrete types.
- Test conditions and variables in the present study differed from those in earlier abrasion test set-ups at NTNU. The repeatability of the abrasion results could therefore not be determined.
- Measurement accuracy increases for greater abrasion depth. It is recommended to ensure a minimum abrasion depth of 0.05 mm.
- Measurement set-up for measuring abrasion depth was repeatable.
- Calculation method 2, referring ice exposed grid points to their nearest reference point, should be used to determine abrasion rate.
- Earlier results showed a linear relation between abrasion rate and sliding distance.
- In accordance with Archard (1953), earlier results showed a linear relation for abrasion rate and contact pressure.

- It is strongly advised to strive towards a measurement and calculation procedure in which an optical surface scanner is implied.
- Concrete roughness does not influence the accuracy of the the measurement set-up.
- Small particles were felt on the concrete sample during abrasion test conduction. Loosing of aggregate stone was not observed.
- Any significant change in concrete profile roughness before and after ice exposure was not observed.
- Surface topography should be investigated with a finer grid mesh, optimally by optical instruments.
- When the volumetric expansion of the ice sample was obstructed, the measured mean abrasion rate was lowest.
- Abrasion as a function of ice porosity seemed to have an influence and should be given more attention.
- Due to ice sample shrinkage (0.61 mm/day), storage in the cold-lab should be avoided.
- If the objective is to investigate the friction coefficient, logging with a high frequency ($\gg 10$ Hz) is recommended.

Bibliography

- Archard, J. (1953). Contact and Rubbing of Flat Surfaces. *Journal of Applied Physics*, 24(8):981–988.
- Ashton, G. D. (2004). *River Lake Ice Engineering*. Water Resources Publications, LCC, P.O. Box, Highlands Ranch, Colorado 80163-0026, USA.
- Bekker, A. T., Gomolskiy, S. G., Sabodash, O. A., Kovalenko, R. G., Uvarova, T. E., Pomnikov, E. E., Prytkov, I. G., and Anokhin, P. (2010). Physical and Mechanical Properties of Modeling Ice for Investigation of Abrasion Process on Ice- Resistant Offshore Platforms. In *Proceedings of the Twentieth (20010) International Offshore and Polar Engineering Conference*, pages 1231–1237. The International Society of Offshore and Polar Engineers.
- Bekker, A. T., Uvarova, T. E., Pomnikov, E. E., and Shamsutdinova, G. R. (2012). Numerical Simulation of Ice Abrasion on Offshore Structures. In *Ice Research for a Sustainable Environment*, pages 897–906. 21st IAHR International Symposium on Ice.
- Bergdahl, L. (1977). Physics of ice and snow as affects thermal pressure. Technical report, Institution för vattenbyggnad, Chalmers Tekniska Högskola.
- Bøhn, O. D. (2011). Ice abrasion of concrete, background and the ntnu laboratory. Master’s thesis, NTNU, Norwegian University of Science and Technology, Faculty of Engineering Science and Technology, Department of Structural Engineering.
- C39, A. I. (2014). Standard test method for compressive strength of cylindrical concrete specimens. Technical report, ASTM International.
- Cole, D. M. (1987). Strain-rate and grain-size effects in ice. *Journal of Glaciology*, 33(115):274–280.
- Cole, D. M. (2001). The microstructure of ice and its influence on mechanical properties. *Engineering Fracture Mechanics*, 68(17-18):1797–1822.
- Cox, G. and Weeks, W. (1983). Equations for determining the gas and brine volumes in sea-ice samples. *Journal of Clacioogy*, 29(102).
- Fiorio, B. (2005). Wear characterisation and degradation mechanisms of a concrete surface under ice friction. *Construction and Building Materials*, 19(5):366–375.

- Fosså, K. T. (2008). Improvement of the ice zone inn structures for sub arctic areas. In *Workshop: Ice Abrasion on Concrete Structures*, pages 1–4. The Nordic Concrete Federation.
- Furukawa, Y. (2011). Ice. In Singh, V. P., Singh, P., and Haritashya, U. K., editors, *Encyclopedia of Snow, Ice and Glaciers*.
- Greaker, N., Pedersen, C. Y., Åse Ervik, Dinzinger, A., and Salganik, E. (2012). Cold lab week 44 report. Report in the course AT-332 at the University Centre in Svalbard, UNIS.
- Greaker, N. S. (2013). Ice quality in measurements of concrete ice abrasion: Pre-study. Project thesis, NTNU, Trondheim.
- Grigalovica, A., Meri, R. M., Zicans, J., Ivanova, T., and Grabis, J. (2013). Exploitation and structural properties of modified polyacetal nanocomposites. In Plank, T. and Pärna, R., editors, *Functional Materials and Nanotechnologies 2013*. FM&NT.
- Gudmestad, O. T. (2013). Oil and gas development in cold climate with emphasis on the barents sea. Lecture notes from the course TBA4265, NTNU.
- Hanada, M., Ujihira, M., Hara, F., and Saeki, H. (1996). Abrasion Rate of Various Material Due to the Movement of Ice Sheets. In *Proceedings of the Sixth (1996) International Offshore and Polar Engineering Conference*, pages 433–437. The International Society of Offshore and Polar Engineers.
- Hara, F., Takahashi, Y., Saeki, H., and Ito, Y. (1995). Evaluation of test methods of abrasion by ice movements on the surface of reinforced concrete structures. In *Proceedings of CONSEC'95: Concrete under Severe Conditions- Environment and loading.*, pages 874–1773. CONSEC.
- Hobbs, P. V. (1974). *Ice Physics*. Oxford University Press Inc., New York.
- Holm, R. (1946). *Electric Contacts*. Hugo Gebers, Stockholm.
- Huovinen, S. (1990). *Abrasion of concrete by ice in arctic sea structures*. Technical Research Center of Finland, Espoo, Finland.
- Itoh, Y., Tanaka, Y., and Saeki, H. (1994). Estimation Method For Abrasion of Concrete Structures Due to Sea Ice Movement. In *Proceedings of the fourth (1994) International Offshore and Polar Engineering Conference*, pages 545–552. The International Society of Offshore and Polar Engineers.
- Itoh, Y., Yoshida, A., Tsuchiya, M., Katoh, K., Corp, T., Sasaki, K., and Saeki, H. (1988). An Eexperimental Study on Abrasion of Concrete Due to Sea Ice. In *Offshore Technology Conference*, pages 61–68.

- Jacobsen, S., Bekker, A., Uvarova, T., Pomnikov, E., Kim, L., and Fosså, K. (2012). Concrete ice abrasion: Deterioration mechanisms, testing and modeling. In *ICDC 2012 - International Congress on Durability of Concrete*. International Congress on Durability of Concrete.
- Jacobsen, S. and Scherer, G. W. (2013). Concrete ice abrasion.
- Jacobsen, S., Scherer, G. W., and Schulson, E. M. (2014). Concrete-Ice Abrasion Mechanics. Submitted to C&CR feb. 5, 2014.
- Jacobsen, S., Sellevold, E. J., Maage, M., Smeplass, S., Kjellsen, K. O., Myrdal, R., Lindgård, J., and Øyvind Bjøntegaard (2013). Effect of temperature. In Jacobsen, S. and Kristoffersen, V., editors, *Betongteknologi 1 (TKT 4215)*.
- Janson, J. E. (1988). Long term resistance of concrete offshore structures in ice environment. In *Proceedings of the 7th International Conference on Offshore Mechanics and Arctic Engineering*, pages 225–231. OMAE.
- Kioka, S. and Takeuchi, T. (2012). Tests on Wear of Various Metals due to Ice Friction. In *Ice Research for a Sustainable Environment*, pages 885–896. 21st IAHR International Symposium on Ice.
- Kirkhaug, J. R. (2013). Ice abrasion and bond testing of repair mortars and high performance concrete. Master's thesis, NTNU, Norwegian University of Science and Technology, Faculty of Engineering Science and Technology, Department of Structural Engineering.
- Lainey, L. and Tinawi, R. (1984). The mechanical properties of sea ice - a compilation of available data. *Canadian Journal of Civil Engineering*, 11(4):884–923.
- Lehmus, E., Kärnä, T., Tanabe, A., Yoshizawa, M., and Sackinger, W. (1997). A comparison of compressive strength of columnar natural sea ice parallel and perpendicular to the c-axis. In *Proceedings of the International Conference on Offshore Mechanics and Arctic Engineering*, pages 251–256. ASME.
- Lyons, L. (1991). *A Practical Guide to Data Analysis for Physical Science Students*. Cambridge University Press, New York.
- Marchenko, A. (2013). Lecture notes. Lecture notes from the course AT-332, UNIS.
- Mitutoyo (2005). *Mitutoyo Digimatic Indicators*.
- Møen, E. (2009). Average abrasion depths for w/c = 0.6 concretes after 500m accumulated sliding. Master's thesis, NTNU, Norwegian University of Science and Technology, Faculty of Engineering Science and Technology, Department of Structural Engineering.
- Norcem (2014). Bestandighetsbrosjyre - god betong er bestandig. Brochure from Norcem AS.

- Palmer, A. and Croasdale, K. (2012). *Arctic offshore engineering*. World Scientific, Singapore.
- Petrovic, J. (2003). Mechanical properties of ice and snow. *Journal of materials science*, 38(1):1–6.
- Saeki, H. (2010). Mechanical properties between ice and various materials used in hydraulic structures: The jin s. chung award lecture, 2010. *International Journal of Offshore and Polar Engineering*, 21(2):81–90.
- Schulson, E. M. and Duval, P. (2009). *Creep and Fracture of Ice*. Cambridge University Press, New York.
- Siengchin, S., Karger-Kocsis, J., Psarras, G. C., and Thomann, R. (2008). Polyoxymethylene/polyurethane/alumina ternary composites: Structure, mechanical, thermal and dielectric properties. *Journal of Applied Polymer Science*, 110(3):1613–1623.
- Sætre, K. (2013). Ice abrasion of concrete - roughness analysis of ice-abraded concrete surfaces using 3d optical scanning. Project thesis.
- Sætre, K. (2014). Laboratory measurements of ice abrasion on different types of fiber reinforced concrete. Master's thesis, NTNU, Norwegian University of Science and Technology, Faculty of Engineering Science and Technology, Department of Structural Engineering.
- Takeuchin, T., Nakazawa, N., Mikami, T., Walanabe, Y., and Saeki, H. (2005). Abrasion of Offshore Structure due to Sea Ice Movement. In *Proceedings of the Fifteenth (2005) International Offshore and Polar Engineering Conference*, pages 729–732. The International Society of Offshore and Polar Engineers.
- Timco, G. and Weeks, W. (2009). A review of the engineering properties of sea ice. *Cold Regions Science and Technology*.

Appendix A

MSc Thesis Template

MASTER DEGREE THESIS

Spring 2014

for

Nicolai Seggaard Greaker

Laboratory Measurements of Ice-Concrete Abrasion with Different Types of Ice Quality

BACKGROUND

There has already been published several papers discussing concrete ice abrasion at NTNU. Much of the work concerns describing and improving the abrasion rig and the involving test and measuring procedures. The importance of concrete and ice parameters on ice-concrete abrasion has been studied and concrete samples with various qualities have been tested. Internationally, research has been carried out for some decades. Literature review shows that the findings in these researches can be contradictory. No standardized test method has been developed for ice abrasion, neither practically nor theoretically. Comparisons of different findings can therefore be challenging, even meaningless. Further knowledge on this topic seems to be needed to draw any solid conclusions. Some interesting findings were uncovered in the earlier thesis "Ice Quality in Measurements of Concrete Ice Abrasion: Pre- study", (Greaker, 2013), which was the pre-study to this thesis. The present work continues and concludes on aspects highlighted in the earlier thesis.

TASK

Task description

- Describe the abrasion rig laboratory as well as the measurement procedures that are going to be applied in this thesis.
- Analyze the abrasion results obtained from different concrete types in earlier theses.
- Investigate the repeatability of the abrasion rig by comparing results from similar experimental set-ups with each other.
- Investigate the possible change of the systems friction coefficient due to a new installed sliding bearing.
- Examine the possible effect volumetric change of ice has on ice-concrete abrasion.
- Investigate the possible effects of different ice qualities on laboratory ice-concrete abrasion tests.

Objective and purpose

The motivation is to determine whether fresh water based laboratory tests can be successfully used as tools to analyze abrasion on marine structures exposed to salt water conditions in extreme environments. The specific objective of this thesis has been to investigate the possible effects of different ice qualities on laboratory ice-concrete abrasion tests. This has been done by altering the ice parameters and keeping other test conditions constant.

General about content, work and presentation

The text for the master thesis is meant as a framework for the work of the candidate. Adjustments might be done as the work progresses. Tentative changes must be done in cooperation and agreement with the professor in charge at the Department.

In the evaluation thoroughness in the work will be emphasized, as will be documentation of independence in assessments and conclusions. Furthermore the presentation (report) should be well organized and edited; providing clear, precise and orderly descriptions without being unnecessary voluminous.

The report shall include:

- Standard report front page (from DAIM, <http://daim.idi.ntnu.no/>)
- Title page with abstract and keywords.(template on: <http://www.ntnu.no/bat/skjemabank>)
- Acknowledgement.
- The main text.
- Text of the Thesis (these pages) signed by professor in charge as Attachment 1.

The thesis can as an alternative be made as a scientific article for international publication, when this is agreed upon by the Professor in charge. Such a report will include the same points as given above, but where the main text includes both the scientific article and a process report.

Advice and guidelines for writing of the report is given in “Writing Reports” by Øivind Arntsen, and in the departments “Råd og retningslinjer for rapportskrivning ved prosjekt og masteroppgave” (In Norwegian) located at <http://www.ntnu.no/bat/studier/oppgaver>.

Submission procedure

Procedures relating to the submission of the thesis are described in DAIM (<http://daim.idi.ntnu.no/>). Printing of the thesis is ordered through DAIM directly to Skipnes Printing delivering the printed paper to the department office 2-4 days later. The department will pay for 3 copies, of which the institute retains two copies. Additional copies must be paid for by the candidate / external partner.

On submission of the thesis the candidate shall submit a CD with the paper in digital form in pdf and Word version, the underlying material (such as data collection) in digital form (e.g. Excel). Students must submit the submission form (from DAIM) where both the Ark-Bibl in SBI and Public Services (Building Safety) of SB II has signed the form. The submission form including the appropriate signatures must be signed by the department office before the form is delivered Faculty Office.

Documentation collected during the work, with support from the Department, shall be handed in to the Department together with the report.

According to the current laws and regulations at NTNU, the report is the property of NTNU. The report and associated results can only be used following approval from NTNU (and external cooperation partner if applicable). The Department has the right to make use of the results from the work as if conducted by a Department employee, as long as other arrangements are not agreed upon beforehand.

Tentative agreement on external supervision, work outside NTNU, economic support etc.

Separate description is to be developed, if and when applicable. See <http://www.ntnu.no/bat/skjemabank> for agreement forms.

Health, environment and safety (HSE) <http://www.ntnu.edu/hse>

NTNU emphasizes the safety for the individual employee and student. The individual safety shall be in the forefront and no one shall take unnecessary chances in carrying out the work. In particular, if the student is to participate in field work, visits, field courses, excursions etc. during the Master Thesis work, he/she shall make himself/herself familiar with "Fieldwork HSE Guidelines". The document is found on the NTNU HMS-pages at <http://www.ntnu.no/hms/retningslinjer/HMSR07E.pdf>

The students do not have a full insurance coverage as a student at NTNU. If you as a student want the same insurance coverage as the employees at the university, you must take out individual travel and personal injury insurance.

Startup and submission deadlines

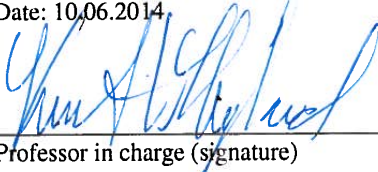
Startup and submission deadlines are according to information found in DAIM.

Professor in charge: Knut Vilhelm Høyland

Other supervisors: Stefan Jacobsen

Department of Civil and Transport Engineering, NTNU

Date: 10.06.2014



Professor in charge (signature)

Appendix B

Ice Samples

Recorded data on all ice samples produced for the experiments conducted in this thesis

Ice Sample #	Procedure #	Freezing Time [days]	Thawing Time [min]	Time Stored [days]
1 - 10		7.9	27	1
11 - 13	1	0.8	24	-
14 - 16		2.9	27	-
17 - 19		3.9	22	-
a15 - a16		7.3	23	1
a18 - a19	2	12.8	30	-
a22 - a23		0.9	28	-
a24 - a26		12.9	25	-
a27 - a29		3.9	20	-
b1 - b3		3	1	33
b4 - b5	2		31	-
b6 - b8	4.8		35	-
b9 - b10	5.8		39	-
b11 - b14	0.8		30	-
c1 - c4	4		1.8	16
c5 - c8		2.1	14	-
c9 -c11		3.9	15	-
c12 - c14		6.6	15	-
c15 -c16		12.7	14	-
c17		4	14	-
See figure A.1		5	7	-

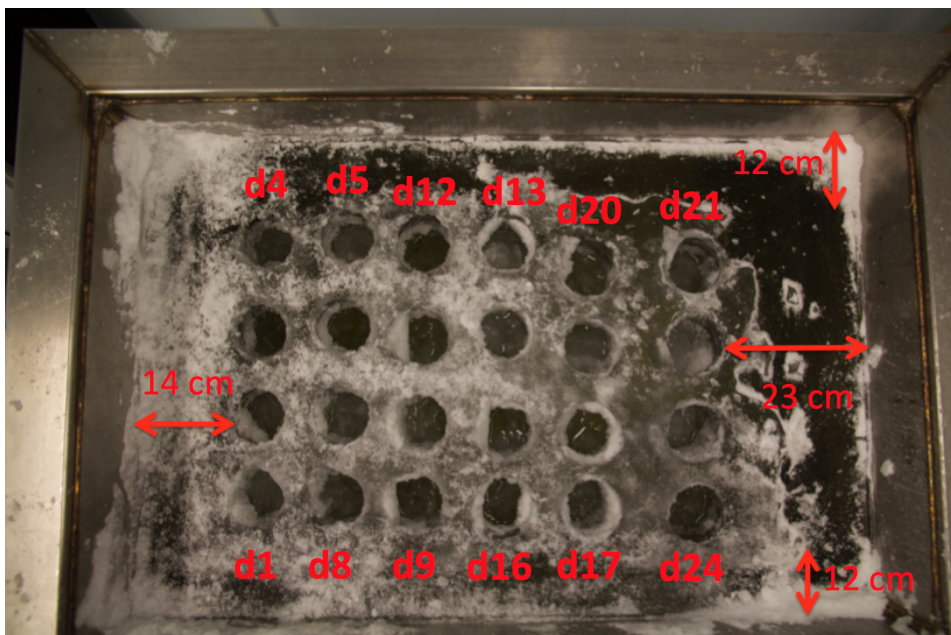


Figure A.1: Origination of ice samples made after procedure 5. View top of FRYIS. Ice thickness \approx 19 cm

Appendix C

Ice Density and Porosity Measurements

Ice density and porosity measurements

Sample #	ρ_{ker} [kg/m ³]	$m_{holder,air}$ [g]	$m_{ice+holder,air}$ [g]	$m_{holder,ker}$ [g]	$m_{ice+holder,ker}$ [g]	Temperature [°C]
Procedure 1 - Pexiglas Tube						
17	762	33.37	602.96	30.42	121.4	-7.7
18	762	33.34	624.7	30.42	124.35	-8.0
19	762	33.33	601.16	30.36	129.05	-7.2
Procedure 2 - POM Tube						
a27	762	33.41	619.05	30.41	123.82	-7.8
a28	762	33.41	648.64	30.45	127.96	-7.7
a29	762	33.43	637.62	30.44	125.98	-7.9
Procedure 3 - Agitated Water						
b12	763	34.4	624.4	30.19	123.29	-1.8
b13	763	34.22	632.55	30.22	124.46	-1.1
b14	763	34.18	602.08	30.28	119.79	-1.6
Procedure 4 - Porous Ice						
c15	762.5	34.4	508.05	30.1	51.75	-6.5
c16	762.5	34.2	492.87	30.13	36.28	-7.0
c17	763.5	34.59	472.78	29.98	33.98	-6.1
Procedure 5 - FRYISIS						
d7	762	33.44	508.14	30.46	110.43	-7.8
d11	762	33.45	553.32	30.46	117.95	-7.6
d21	762	33.46	571.86	30.46	121.05	-7.8

Appendix D

Concrete Density Measurement

Mass, m_{con} and submerged mass, $m_{con,s}$ for the concrete samples used to determine their densities.

m_{con} [g]	$m_{con,s}$ [g]
3413.8	1900.3
3367.9	1876.1
3388.0	1871.8
3270.3	1871.8

Appendix E

Mean Abrasion Rates from earlier Results

Mean abrasion rate, μ calculated from equation 1.35 in Lyons (1991). Data based on earlier results found by Kirkhaug (2013) and Møen (2009)

Concrete Specimen	Student	μ [mm/km]
<hr/>		
Sliding velocity = 0.16 cm/s and Contact Pressure = 1 MPa		
w/c = 0.6 w/ air	Møen	0.08
Reforcetech	Kirkhaug	0.03
Densit		0.0248
Densit Sandb.		0.022
B70		0.0503
B60		0.0895
B60 Sandblasted		0.0715
Rockbond		0.0403
<hr/>		
Sliding velocity = 0.25 cm/s and Contact Pressure = 1 MPa		
Reforcetech	Kirkhaug	0.0265
Densit		0.0143
B70		0.0385
B60		0.078
Rockbond		0.0345
<hr/>		
Sliding velocity = 0.16 cm/s and Contact Pressure = 0.5 MPa		
Reforcetech	Kirkhaug	0.017
Densit		0.031
B70		0.0243
B60		0.0293
Rockbond		0.0235

Appendix F

Abrasion Depth Measurement Sheet

X/Y	Avstand abraderet:										Dato:	
	-100	-80	-60	-40	-20	0	20	40	60	80		100
5												
10												
22												
32												
42												
52												
62												
72												
82												
94												
99												

Abrasion depth measurement sheet. X-axis is as in figure 3.16. Sheet was made by Kristian Sætre, (Sætre, 2014). Translation of text: Sample, distance abraded and date.

Appendix G

Ice-Concrete Abrasion Chart

Conducted ice-concrete abrasion tests during spring 2014. Ice samples were used in corresponding order.

Concrete Sample	Ice Samples	Date
STD9	1, 2, 3	9/4
STD12	4, 5, 6	9/4
STD 6	11, 12	25/4
D4	a15, a16	9/4
D1	a18, a19	21/4
D8.2	a22, a23	22/4
D8	b1, b2	24/4
D2.2	b4, b5, b3	25/4
D2	b6, b7, b8	28/4
D7.2	c1, c2, c3	30/4
D6.2	c4, c5, c6, c7, c8	30/4
D7	c9, c10, c11	4/5
D1.2	d10, d6	10/5
D6	d14, d12	10/5
D4.2	d17, d15	10/5

Appendix H

Matlab Script for Abrasion Result Presentation

```
function [] = ABRASION(Directory)
```

```
close all  
clc
```

ABRASION RIG FRICTION v.1

```
%NB: This version of the script can only compute up to 4 .txt files
```

Set Up

```
% - Script is stored in the preceding folder of the data which will be  
% analysed  
% - Data must be logged in Hz.
```

Instructions

```
% 1) Open .txt file from Isabrasive-v3 with an editor of choice  
% 2) Replace all ',,' with '.'  
% 3) Delete titles  
% 4) Save .txt file as 'data*'; where * is 1,2,3...,n-files  
% 5) Drag .txt file to Matlab Workspace  
% 6) Import as Matrix (.mat)  
% 7) Create folder named after the sample (only sperate with _ or -)  
% 8) Save .mat file  
% 9) Repeat for all .txt files
```

Data Import

```
% Chooses directory containing .mat-files to import

cd(sprintf('%s',Directory))

currentDirectory = pwd ;
[upperPath, str, ~] = fileparts(currentDirectory) ;

files = dir('*.mat');
for nm=1:length(files);
    load(['data',num2str(nm),'.mat']);
end

cd ../
```

Data Compilation

```
% num*(:,1) = Log Time [s]
% num*(:,2) = Friction Hz
% num*(:,3) = Horizontal Position Hz
% num*(:,4) = Load [N]
% num*(:,5) = Room Temperature [C]

count = 1;

if nm >= count ;

num1 = zeros(length(data1),3);
for i=1:length(data1);
    num1(i,1) = data1(i,3);
    num1(i,2) = data1(i,16);
    num1(i,3) = data1(i,6);
    num1(i,4) = data1(i,9);
    num1(i,5) = data1(i,21);
end

DATA = num1;

end

count = count+1;

if nm >= count ;

num2 = zeros(length(data2),3);
```

```

for i=1:length(data2);
    num2(i,1) = data2(i,3) + num1(length(num1),1);
    num2(i,2) = data2(i,16);
    num2(i,3) = data2(i,6);
    num2(i,4) = data2(i,9);
    num2(i,5) = data2(i,21);
end

DATA(length(num1)+1:length(num1)+length(num2),1) = num2(:,1);
DATA(length(num1)+1:length(num1)+length(num2),2) = num2(:,2);
DATA(length(num1)+1:length(num1)+length(num2),3) = num2(:,3);
DATA(length(num1)+1:length(num1)+length(num2),4) = num2(:,4);
DATA(length(num1)+1:length(num1)+length(num2),5) = num2(:,5);

end

count = count+1;

if nm >= count ;

num3 = zeros(length(data3),3);
for i=1:length(data3)
    num3(i,1) = data3(i,3) + num2(length(num2),1);
    num3(i,2) = data3(i,16);
    num3(i,3) = data3(i,6);
    num3(i,4) = data3(i,9);
    num3(i,5) = data3(i,21);
end

DATA(length(num1)+length(num2)+1:length(num1)...
+length(num2)+length(num3),1) = num3(:,1);
DATA(length(num1)+length(num2)+1:length(num1)...
+length(num2)+length(num3),2) = num3(:,2);
DATA(length(num1)+length(num2)+1:length(num1)...
+length(num2)+length(num3),3) = num3(:,3);
DATA(length(num1)+length(num2)+1:length(num1)...
+length(num2)+length(num3),4) = num3(:,4);
DATA(length(num1)+length(num2)+1:length(num1)...
+length(num2)+length(num3),5) = num3(:,5);

end

count = count+1;

if nm >= count ;

```

```

num4 = zeros(length(data4),3);
for i=1:length(data4)
    num4(i,1) = data4(i,3) + num3(length(num3),1);
    num4(i,2) = data4(i,16);
    num4(i,3) = data4(i,6);
    num4(i,4) = data4(i,9);
    num4(i,5) = data4(i,21);
end

DATA(length(num1)+length(num2)+length(num3)+1:length(num1)+length(num2)...
+length(num3)+length(num4),1) = num4(:,1);
DATA(length(num1)+length(num2)+length(num3)+1:length(num1)+length(num2)...
+length(num3)+length(num4),2) = num4(:,2);
DATA(length(num1)+length(num2)+length(num3)+1:length(num1)+length(num2)...
+length(num3)+length(num4),3) = num4(:,3);
DATA(length(num1)+length(num2)+length(num3)+1:length(num1)+length(num2)...
+length(num3)+length(num4),4) = num4(:,4);
DATA(length(num1)+length(num2)+length(num3)+1:length(num1)+length(num2)...
+length(num3)+length(num4),5) = num4(:,5);

end

x = DATA(:,1); % Log Time [s]
y1 = DATA(:,2); % Friction Hz
y2 = DATA(:,3); % Horizontal Position Hz
F = DATA(:,4)/1000; % Load [kN]
T = DATA(:,5); %Temperature [C]

```

FRITION: Figure Handling and Interval Selection

```

figure('name','Postion and Friction','Units','centimeters','position',...
[5 5 35 18]);
[AX, L1, L2] = plotyy(x,y1,x,y2);

title(str,'FontSize',25)
xlabel('Time (sec.)','FontSize',25)
set(get(AX(1),'Ylabel'),'String','Friction Coef.','FontSize',25)
set(get(AX(2),'Ylabel'),'String','Hor. Position (mm)','FontSize',25)

set(AX(1), 'ylim', [-0.3 0.3]) % Handle 'Friction coef.' Axis
set(AX(2), 'ylim', [min(y2)-5 max(y2)+5]) % Handle 'Hor. Pos.' Axis
set(AX(1), 'xlim', [0 max(x)]) % Handle X-Axis
set(AX(2), 'xlim', [0 max(x)])

set(AX(1),'YTick',-0.3:0.1:0.3,'FontSize',20) % Handle 'Friction coef.' Ticks

```

```

set(AX(2),'YTick',-120:20:100,'FontSize',20) % Handle 'Hor. Pos.' Ticks

set(AX(1),'XTick',600:600:length(x),'XTickLabel',[600:600:length(x)]/60)
set(AX(2),'XTick',600:600:length(x),'XTickLabel',[600:600:length(x)]/60)
set(L2,'LineStyle',':') % Choose 'Friction coef.' Linestyle

set(gcf,'Color',[1 1 1]) % Background color

%Select Intervals

\begin{verbatim}
f1=gcf;
f2=figure('name','After 30 min','Units','centimeters','position',[5 5 29 18]);
copyobj(get(f1,'children'),f2);

hf = get(gcf,'Children');
set(hf,'xlim', [1800 1825],'XTick',1:10:length(x),'XTickLabel',1:10:length(x))
h_str=get(hf(2),'Title');
title_30 = strcat(str,{''; after 30 min of ice sliding'});
set(h_str,'String',title_30);

set(gcf,'Color',[1 1 1])

% Next Interval
f3=figure('name','After 1 hour','Units','centimeters','position',[5 5 29 18]);
copyobj(get(f1,'children'),f3);

hf = get(gcf,'Children');
set(hf,'xlim', [3600 3625],'XTick',1:10:length(x),'XTickLabel',1:10:length(x))
h_str=get(hf(2),'Title');
title_60 = strcat(str,{''; after 1 hour of ice sliding'});
set(h_str,'String',title_60);

set(gcf,'Color',[1 1 1])

% Next Interval
f4=figure('name','After 2 hour','Units','centimeters','position',[5 5 29 18]);
copyobj(get(f1,'children'),f4);

hf = get(gcf,'Children');
set(hf,'xlim', [7200 7225],'XTick',1:10:length(x),'XTickLabel',1:10:length(x))
h_str=get(hf(2),'Title');
title_120 = strcat(str,{''; after 2 hour of ice sliding'});
set(h_str,'String',title_120);

```

```

set(gcf,'Color',[1 1 1])

%Only Friction vs. Time
f5=figure('name','Friciton','Units','centimeters','position',[5 5 35 18]);
plot(x,y1)
xlabel('Time (sec.)','FontSize',25)
ylabel('Friction coef.','FontSize',25)
title_friction = strcat(str,'- Friction coef. Full Test');
title(title_friction,'FontSize',25)
xlabel('Time (min.)','FontSize',25)
axis([0 max(x) -0.5 0.5])

set(gcf,'Color',[1 1 1])
set(gca, 'XTickLabel',[600:600:length(x)]/60, ...
'XTick',600:600:length(x),'FontSize',20, ...
'YTick',-0.5:.1:0.5)

```

Load

```

Mean_P = sprintf('%.2f',mean(F)*1000/4231.4);
f6=figure('name','Load','Units','centimeters','position',[5 5 35 22]);
plot(x,F)
xlabel('Time (min.)','FontSize',25)
ylabel('Load [kN]','FontSize',25)
title_load = strcat(str,'- Load vs. Time');
title([title_load ; sprintf('%s','Mean Contact Pressure: ', ...
num2str(Mean_P),'MPa')],'FontSize',25)
axis([0 max(x) min(F)+3 max(F)+0.5])

set(gcf,'Color',[1 1 1])
set(gca,'XTickLabel',[600:600:length(x)]/60, 'XTick',600:600:length(x),...
'FontSize',20)

```

Air Temperature

```

Mean_T = sprintf('%.2f',mean(T));

f7=figure('name','Temperature','Units','centimeters','position',[5 5 35 22]);
plot(x(1:600:end),T(1:600:end),'LineWidth',3) %plot each minute
xlabel('Time (min.)','FontSize',25)
ylabel('Temperature [^\circ C]','FontSize',25)
title_temp = strcat(str,'- Room Temperature vs. Time');
title([title_temp;; sprintf('%s','Mean Temperature: ',...
num2str(Mean_T),' ^\circ C')],'FontSize',25)
axis([0 max(x) min(T)-1 max(T)+1])

```

```
set(gca, 'XTickLabel',[600:600:length(x)]/60, ...  
'XTick',600:600:length(x),'FontSize',20)  
set(gcf,'Color',[1 1 1])
```

Figure Export

```
% In order to auto-save figures; download export_fig from:  
% http://www.mathworks.com/matlabcentral/fileexchange/23629-exportfig  
% Follow their instructions
```

```
end
```